Accepted Manuscript

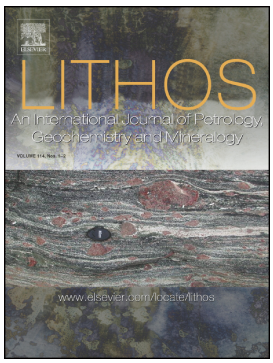

Petrogenesis and metallogenesis of the Wajilitag and Puchang Fe-Ti oxide-rich intrusive complexes, northwestern Tarim Large Igneous Province

Dongyang Zhang, Zhaochong Zhang, He Huang, Zhiguo Cheng, Bernard Charlier

PII: S0024-4937(18)30067-7
DOI: doi:10.1016/j.lithos.2018.02.019
Reference: LITHOS 4578

To appear in:

Received date: 28 October 2017
Accepted date: 18 February 2018

Please cite this article as: Dongyang Zhang, Zhaochong Zhang, He Huang, Zhiguo Cheng, Bernard Charlier , Petrogenesis and metallogenesis of the Wajilitag and Puchang Fe-Ti oxide-rich intrusive complexes, northwestern Tarim Large Igneous Province. The address for the corresponding author was captured as affiliation for all authors. Please check if appropriate. Lithos(2018), doi:10.1016/j.lithos.2018.02.019

Petrogenesis and metallogenesis of the Wajilitag and Puchang Fe-Ti oxide-rich intrusive complexes, northwestern Tarim Large Igneous Province

Dongyang Zhang[a,b], Zhaochong Zhang[a]*, He Huang[c], Zhiguo Cheng[a], Bernard Charlier[d,e]

[a] State Key Laboratory of Geological Processes and Mineral Resources, China University of Geosciences, Beijing 100083, China

[b] State Key Laboratory of Geological Processes and Mineral Resources, China University of Geosciences, Wuhan 430074, China

[c] Institute of Geology, Chinese Academy of Geological Sciences, Beijing 100037, China

[d] Institut für Mineralogie, Leibniz Universität Hannover, Hannover 30167, Germany

[e] Department of Geology, University of Liège, 4000 Sart Tilman, Belgium

* Corresponding author. Zhaochong Zhang, School of Earth Sciences and Mineral Resources, China University of Geosciences, No. 29 Xueyuan Road, Beijing, 100083, P.R. China. Tel: +86 10 8232 2195 Fax: +86 10 82323419. *E–mail addresses*: zczhang@cugb.edu.cn (ZC Zhang).

ABSTRACT

The Wajilitag and Puchang intrusive complexes of the Tarim large igneous province (TLIP) are associated with significant resources of Fe–Ti oxide ores. These two mafic–ultramafic intrusions show differences in lithology and mineral chemistry. Clinopyroxenite and melagabbro are the dominant rock types in the Wajilitag complex, whereas the Puchang complex is generally gabbroic and anorthositic in composition with minor plagioclase–bearing

clinopyroxenites in the marginal zone. Disseminated Fe–Ti oxide ores are found in the Wajilitag complex and closely associated with clinopyroxenites, whereas the Puchang complex hosts massive to disseminated Fe–Ti oxide ores mainly within its gabbroic rocks. The Wajilitag intrusive rocks are characterized by a restricted range of initial $^{87}Sr/^{86}Sr$ ratios (0.7038–0.7048) and positive $\varepsilon_{Nd}(t)$ (+0.04–+3.01), indicating insignificant involvement of continental crustal contamination. The slightly higher initial $^{87}Sr/^{86}Sr$ ratios (0.7039–0.7059) and lower $\varepsilon_{Nd}(t)$ values (–1.05–+2.35) of the Puchang intrusive rocks also suggest that the isotopic characteristics was controlled primarily by their mantle source, rather than by crustal contamination. Both complexes have Sr–Nd isotopic compositions close the neighboring kimberlitic rocks and their hosted mantle xenoliths in the TLIP. This indicates that the ferrobasaltic parental magmas were most probably originated from partial melting of a metasomatized subcontinental lithospheric mantle, modified recently with subduction–related materials by the impingement of the ascending mantle plume. The recycled subduction–related materials preserved in the lithospheric mantle could play a key role in the formation of the parental Fe–rich magmas in the context of an overall LIP system. The distinct variations in mineral assemblage for each complex and modeled results indicated that the Wajilitag and Puchang complexes experienced different crystallization path. Fe–Ti oxides in Wajilitag joined the liquidus earlier in the crystallization sequence, especially relative to the crystallization of plagioclase. This is attributed to the relatively high TFeO, TiO_2 and initial H_2O contents of the parental magma. In combination with definitive field and petrological evidence, the enrichment of highly incompatible elements (e.g., Zr, Hf, Nb and Ta) and the depletion of rare earth elements in the Fe–Ti oxide ores is consistent with the plausible interpretation that the ores could be formed by fractional crystallization and crystal accumulation of the Fe–Ti oxide crystals from the ferrobasaltic parental magmas. A considerable amount of the Fe–Ti oxides in the Puchang has transported and sunk from higher up in the

chamber to the underlying unconsolidated silicate crystal pile. The highly dense Fe–Ti oxide crystal slurries further tended to effective accumulate Fe–Ti oxides to form high–grade Fe–Ti oxide ore bodies, and subsequent rapid collapse and intrusive into lower lithologies within the complex under a H_2O–rich environment during the late–stage of magmatic differentiation. The development of massive Fe–Ti oxide ores in the case of the Puchang, could plausibly result from a combination of the protracted differentiation history of a Fe highly enriched parental magma and the later addition of external H_2O from the country rocks (e.g., carbonates) to the slowly cooling magma chamber.

Key words: Fe–Ti oxide ores; igneous complex; ferrobasalt; fractional crystallization; Tarim large igneous province

1. Introduction

The metallogenic potential of some plume–related large igneous provinces (LIPs) have received considerable attention, partly because of major resources for Cu–Ni–Platinum group element (PGE) and Fe–Ti–V oxide ores (Ernst and Jowitt, 2013). Numerous recent studies have focused on the formation of the Fe–Ti–V oxide ores (magnetite ± ilmenite). This ore type is particularly abundant in the Emeishan LIP and ore-forming processes have been intensively debated. Two radically different hypotheses are proposed: (1) crystallization of a distinct Fe–Ti±P rich immiscible liquid segregated from the evolved basaltic magma (Liu et al., 2014 and references therein), and (2) early crystallization and gravitational accumulation of the Fe–Ti–V oxide crystals from the ferrobasaltic or ferropicritic parental magmas (Pang et al., 2008a, 2008b; Zhang et al., 2009). In the latter genetic model, some fundamentally different formation processes, including frequent Fe–Ti–enriched magma replenishment in a complex magma plumbing system (Bai et al., 2012; Song et al., 2013) and change in water, pressure and oxygen fugacity (fO_2) conditions

(Ganino et al., 2008; Howarth et al., 2013) have been proposed for the concentration of oxides from magmas. Accordingly, the study of mechanisms for the enrichment of Fe–Ti oxide ore in mafic–ultramafic intrusions continues to be a relevant and controversial topic (Tang et al., 2017).

Large volumes of early Permian volcanic rocks have recently been identified in the Tarim Craton and adjacent areas in the northwestern China, constituting a new LIP (Li et al., 2012b; Tian et al., 2010), comparable to the ~251 Ma Siberian Traps in Russia (Prokoph et al., 2013), the ~260 Ma Emeishan Large Igneous Province (ELIP) in southwestern China (Shellnutt, 2014), and the ~289 Ma Panjal Traps of Kashmir (Shellnutt et al., 2011) (Fig. 1a). At the moment little is known about the metallogenesis in the recently recognized Tarim large igneous province (TLIP). Fortunately, the newly identified Wajilitag and Puchang Fe–Ti oxide ore–bearing intrusive complexes in the northwestern TLIP (Fig. 1b) provide an excellent case study to assess the links between magma evolution and Fe–Ti ore formation. Although preliminary studies suggested that both complexes are parts of the TLIP (Cao et al., 2014; Li et al., 2012a; Zhang et al., 2008, 2010), the critical data required to study the genetic relationship between mantle source and ore genesis, and the large–scale magma chamber processes associated with the concentration of Fe–Ti oxides in the mafic–ultramafic complexes, remain unclear. Recent drilling and active open pit operations in the two complexes constitute an excellent opportunity to carry out more systematic investigations and sampling.

In this contribution, we present careful field and petrological investigation, Sr–Nd isotopic data of whole rocks and clinopyroxene separates, whole rock major and trace elemental and mineral composition data for the Wajilitag and Puchang intrusive rocks and associated Fe–Ti oxide ores. Samples are from two drillcores and surface exposures. All these results, combined with previous available petrochemical data, contribute to a better understanding of the nature and origin of the parental magmas and the differentiation processes of the crustal magma chamber, and constrain the potential link between plume-plate

interaction and metallogenesis in the TLIP, and the formation of massive Fe–Ti oxide ores in ferrobasaltic systems.

2. Geological background

2.1. Regional geology

The Tarim Craton of NW China is bounded by the Tianshan orogen to the north and west, the Kunlun orogen to the south and Altyn Tagh orogen to the southeast (Fig. 1b). It consists of a Precambrian crystalline basement overlain by a thick sequence of Phanerozoic shallow marine and terrestrial sandstones, siltstones, shales, dark limestones, chert and volcanic rocks (Zhang et al., 2012a). Recent studies have revealed several episodes of tectono–thermal events associated with the craton, including late Neoarchean to early Paleoproterozoic, late Paleoproterozoic to early Neoproterozoic, Silurian to Devonian and Permian events in different regions (Long et al., 2011; Zhang et al., 2012a). Among them, the Permian magmatic event related to the Tarim LIP (Fig. 1b) is probably the largest one in terms of its magnitude and spatial distribution (Xu et al., 2014 and references therein).

The TLIP is composed of voluminous volcanic successions consisting primarily of alkaline basalts with minor picrites, andesites, dacites and rhyolites. They range from several hundred meters to 3.0 km thick with an estimated average thickness of ~1 km, suggesting a volume of more than 300,000 km^3 (Tian et al., 2010). This huge magmatic event is believed to have resulted from a mantle plume activity (Li et al., 2012b; Xu et al., 2014; Zhang et al., 2013).

Numerous intrusive bodies are closely associated with the Tarim flood basalts (Huang et al., 2012; Li et al., 2012b). These intrusions range from ultramafic and mafic to felsic compositions. Among them, the Wajilitag and Puchang complexes exposed in the northwestern TLIP have been recently identified to host orthomagmatic Fe–Ti oxide deposits (Figs. 1b, 2and 3).

2.2. Geology and petrography of Wajilitag and Puchang complexes

2.2.1. Wajilitag complex

The Wajilitag intrusive complex is ~5.0–km long, 1.5–3.0–km wide, with an exposed area of ~12 km^2 near the Bachu town (Figs. 1b and 2a). It was dated using SIMS and LA–ICP–MS U–Pb zircon methods at ca. 283 Ma (Zhang et al., 2016). The vertical downward extension of the complex exceeds 1 km by current deep drill holes. If and how the complex opens at depth has not been determined, because the lower contact with the country rocks has not been intersected by drill–cores (Fig. 2b and c). It intruded the flat–lying and metamorphosed continental clastic sequences of the Devonian Kezi'ertag and Yimugantawu formations, and is covered by Neogene aeolian sediments. The complex was cut through by some syenite bodies (Fig. 2a), which have been suggested to represent evolved residual liquids left after extensive fractionation of the mafic–ultramafic suite from the Wajilitag parental magma (Zhang et al., 2008). The complex consists predominantly of clinopyroxenite and melagabbro with gradational contacts. No prominent igneous lineation or layering is observed in the complex. Fe–Ti oxide mineralization is concentrated in clinopyroxenite, and some Fe–Ti oxide ore bodies are present close to the transition between clinopyroxenite and melagabbro (Fig. 2). The ore bodies occur as irregular lens and dyke–shaped. To date, only disseminated Fe–Ti oxide ores have been identified in the complex (25–80 vol.% Fe–Ti oxides). The contacts between the disseminated ore bodies and the adjacent silicate rocks are commonly transitional. According to a report released in 2010 by Xinjiang Bayi Iron and Steel Ltd. (now part of Baosteel Group), the complex contains 146 million tons (Mt) of ore reserves with an average grade of ~17 wt.% total FeO (TFeO) and ~7 wt.% TiO_2.

The clinopyroxenite has fine– to medium–grained texture with local coarse–grained facies. The rock generally contains 70–80 vol.% cumulus clinopyroxene, and 10–20 vol.% Fe–Ti oxides (both magnetite and ilmenite,

hereinafter) with a few percent of plagioclase (Table 1; Figs. 4a and 5a). Some samples (e.g., ZK4503–9) also contain abundant cumulus olivine (up to 20 vol.%). Euhedral to subeuhedral olivine may occur with clinopyroxene (Figs. 4b and 5b). Plagioclase is occasionally interstitial to clinopyroxene (Fig. 5a). For simplicity, the term clinopyroxenite is used to denote these lithological units throughout this study. The melagabbro is composed mainly of fine– to medium–grained clinopyroxene (30–60 vol.%), plagioclase (20–40 vol.%), Fe–Ti oxides (5–15 vol.%; Fig. 4c). Some melagabbro samples (e.g., ZK4503–21; Table 1) also contain small amounts (up to vol.5%) of olivine (Fig. 5c) and rarely up to 60 vol.% plagioclase (e.g., DW33–1) (Fig. 4d). Porphyritic texture is present in some gabbroic samples characterized by highly variable sizes of olivine and clinopyroxene crystals (Fig. 4e). The disseminated ore (25–80 vol.% Fe–Ti oxides) in the Wajilitag is commonly fine to medium grained and typically is composed of 25–50 vol.% magnetite, 30–50 vol.% clinopyroxene and 10–15 vol.% ilmenite, plus small amounts of olivine, interstitial plagioclase (Fig. 4f). Minor base–metal sulfides (e.g., pyrrhotite) also occur in the interstitial phase in silicates and oxides.

It is noteworthy that some euhedral and rounded Fe–Ti oxide grains enclosed in the silicate minerals may represent primocrysts that were crystallized together and trapped within the silicate crystals from the same magma (Pang et al., 2008a). Magnetite grains commonly contain trellis and sandwich ilmenite lamellae or rims, whereas most ilmenite crystals in the studied samples are relatively homogeneous (Figs. 5a and b).

2.2.2. Puchang complex

The Puchang (or Piqiang in some literature) intrusive complex is exposed ~120 km northeast of the Atushi city (Fig. 1b). Zircon U–Pb dating results indicate that the complex formed at ca. 275 Ma (Zhang et al., 2010, 2016). The complex has an outcrop area of ~25 km^2, and intrudes the lower Carboniferous Kangkelin Formation, which consists mainly of calcareous slate and marble

(Figs. 3a and 6a). Late mafic and felsic dykes of variable sizes and strikes intersected the complex in many locations. It is covered by Neogene sedimentary rocks in the western and eastern portions. The floor of the complex has not been reached by current mining and the deep drill holes (Fig. 3b and c). The complex is composed of plagioclase–bearing clinopyroxenite, gabbro and anorthosite, of which gabbro is the predominant component. The plagioclase–bearing clinopyroxenite is mainly distributed at the margins of the complex, and the anorthositic rock forms small separated cupolas topping some parts of the complex (Fig. 3a). Gabbroic rocks can be subdivided into medium–grained ore–barren gabbro and fine–grained oxide gabbro (mostly referred as disseminated ore in this study). It must be noted that no distinct boundaries among clinopyroxenitic, barren gabbroic and anorthositic suites can be recognized, whereas the oxide gabbros exceptionally show clear sharp contact with the barren gabbros (Fig. 6b). Most barren silicate rocks display no modal igneous layering and appear extremely homogeneous in outcrop, but oxide gabbros locally exhibit well–defined layering. Many centimeter– to decimeter–scale marble xenoliths occur in the clinopyroxenite close to the most external part of the contact zone between the clinopyroxenite and the country rocks.

The Fe–Ti oxide ore bodies mainly have the morphology of irregular lenses, layers or tabular horizons, and generally display sharp boundaries with or within the gabbric rocks (Fig. 3). Both massive and disseminated Fe–Ti oxide ore bodies also have sharp contacts with each other (Fig. 6c). Centimeter–scale massive ore bands appear in disseminated ore bodies (Fig. 6d). Most layers are generally ca. 50 cm thick but may range from a few centimeters to ~0.8 cm (Fig. 6e). According to field observations, most, if not all, ore bodies have a prominent layered structure. Detailed exploration by the No.2 Geological Party of Xinjiang Bureau of Geology and Mineral Resources has shown that ore reserves have been estimated at 120 Mt with an average grade of ca. 20 wt.% TFeO and ca. 11 wt.% TiO_2.

The fine– to medium–grained plagioclase–bearing clinopyroxenite predominantly consists of clinopyroxene (~90 vol.%) and interstitial plagioclase (~5 vol.%), with minor Fe–Ti oxides (Table 1). Some plagioclase crystals in clinopyroxenite have been partially or completely altered to albite. However, the majority of rocks are unaltered. The most striking characteristic of the clinopyroxene grains is their straight boundaries with distinct ~120° triple junctions (Fig. 6f). The gabbro is mediume– to coarse–grained and composed of plagioclase (20–75 vol.%) and clinopyroxene (10–40 vol.%), with a few percent of Fe–Ti oxides (5–15 vol.%; Fig. 6g). In some plagioclase–rich gabbro samples, planar foliation and lineation are shown by platy orientation of long lath–shaped plagioclase and small subhedral to euhedral prismatic clinopyroxene (Fig. 6g). Several gabbroic samples (e.g., ZK4–2–9–1, ZK4–2–22–2 and NPC–11) contain up to 25 vol.% cumulus olivine in addition to the above minerals (Fig. 6h). The anorthosite is medium– to coarse–grained rocks with ~90 vol.% cumulus plagioclase, ~3 vol.% olivine and ~2 vol.% clinopyroxene (Table 1), and Fe–Ti oxides. Some clinopyroxene grains are observed as coronitic rims around olivine and plagioclase in some anorthositic samples (Fig. 6i). In some cases, plagioclase occurs as euhedral grains and it is lobate with evidence of high temperature deformation features (e.g., kinked band), likely resulting from compaction of the crystal pile. Disseminated ore is fine to medium grained and consists of 25–45 vol.% Fe–Ti oxides, 25–40 vol.% plagioclase and 10–25 vol.% clinopyroxene, with small amounts of olivine, and hornblende rim (Fig. 6j). Ores containing >80 vol.% Fe–Ti oxides are referred to as massive ores in this study. Most massive ore samples in the Puchang also contain small amounts of silicates dominated by plagioclase and lesser olivine, clinopyroxene and sulfides with reaction rims of hornblende (Fig. 6k–l).

The Fe–Ti oxides occur as anhedral grains and are dominated by magnetite with subordinate ilmenite. Similarly, euhedral and sub–rounded Fe–Ti oxide grains have locally been observed as inclusions in silicate minerals (Fig. 7) It is noteworthy that plagioclase, olivine and clinopyroxene

grains within the Puchang oxide ores are typically embayed/resorbed and have distinct reaction rims of hornblende, indicating disequilibrium textures between oxides and coexisting silicates. The oxide ore samples (in particular massive ores; Fig. 5j, k) contain much more interstitial hornblende than the Wajilitag ores.

3. Sampling and analytical methods

In this study, we have selected 64 unaltered or the least altered samples: 30 from the Wajilitag and 34 from the Puchang complexes. Most samples were collected from two drilled boreholes (borehole numbers ZK4503 and ZK4–2), completed by surface sampling. Their locations are indicated in Figs. 2 and 3, and coordinates are reported in Table 1. The exposed portions and weathered surfaces of the samples were carefully removed and polished thin sections were made from all samples. The fresh interior pieces of the samples were crushed into very fine powders using an agate disintegrator at the Institute of Regional Geology and Resource Survey, Langfang, Hebei Province, China. Clinopyroxene grains were separated by standard density and magnetic separation procedures and hand–picking under a binocular microscope for Sr–Nd isotope analysis.

3.1. Mineral chemistry

Mineral compositions were determined using an EPMA–1600 electron microprobe and a JEOL–JXA8230 microprobe with four wavelength dispersive spectrometers at the State Key Laboratory of Geological Processes and Mineral Resources, University of Geosciences (Beijing) and the MLR Laboratory of Metallogeny and Mineral Assessment, Institute of Mineral Resources, Chinese Academy of Geological Sciences (CAGS) in Beijing, respectively. Back–scattered electron (BSE) images were conducted using the same instrument. Some olivine and clinopyroxene grains were analyzed along profiles to examine intra–grain compositional variations. Standard operating

conditions were excitation voltage of 15 kV and beam current of 10 nA. Peak and background counting times were set at 30 and 15 s, respectively. The spot diameter was 5 μm in most cases, but a focused beam of 2μm was also used. Matrix effects were corrected with the ZAF software. The accuracy of analyzes was monitored using mineral standards and analytical reproducibility was within 2 wt.% error. Ferrous and ferric iron in minerals were estimated from stoichiometry and charge balance.

3.2. Major and trace element contents

Bulk–rock major oxides were analyzed at the Institute of Geology and Geophysics, Chinese Academy of Sciences with an X–ray fluorescence spectrometer (Shimadzu XRF–1500) using fused glass discs. The FeO concentration was determined using a conventional wet chemical titration procedure. The loss on ignition (LOI) was measured after 1 h baking at 1000 °C. The analytical precisions for major oxides based on certified standards (GSR–1, GSR–3) and duplicate analyzes expressed in terms of relative percentages range from ±0.01 wt.% to ±0.20 wt.%. Whole rock trace elements were analyzed by ICP–MS at the National Research Center of Geoanalyzis, CAGS, using the analytical procedure described by Qi et al. (2000). For trace element analysis, three Chinese national standard reference materials (GBW07105, GBW07108 and GBW07111; Supplementary Data Electronic Appendix 1) were used for quality control. The precision is generally better than 5% for trace elements.

3.3. Sr–Nd isotopic analyses

Sr–Nd isotope compositions of whole rock samples marked with an asterisk (*) were analyzed using a VG354 mass spectrometer at the Center of Materials analysis, Nanjing University, whereas those of the remaining whole rocks and clinopyroxene separates were determined on a MAT262 mass spectrometer at Institute of Geology, CAGS. Details on the chemical procedures were described by Zhang et al. (2012c) and Chen et al. (2002),

respectively. Total procedure blanks per analysis were <100 pg for Sm and Nd and <50 pg for Rb and Sr. $^{87}Sr/^{86}Sr$ ratios were normalized to $^{86}Sr/^{88}Sr=0.1194$, with uncertainties indicated as 2σ. $^{143}Nd/^{144}Nd$ ratios were normalized to $^{146}Nd/^{144}Nd=0.7219$ and uncertainties were expressed as 2σ. Four measurements on the Sr standard NBS987 and two Nd standard LaJolla and JMS gave $^{86}Sr/^{88}Sr=0.710236\pm7$ (2σ), 0.710242 ± 1 (2σ) and $^{143}Nd/^{144}Nd=0.511862\pm6$ (2σ), 0.511128 ± 10 (2σ), respectively, during the period of data acquisition. The initial $^{87}Sr/^{86}Sr$ ratios (I_{Sr}) and $\varepsilon_{Nd}(t)$ values are calculated based on modern $(^{87}Rb/^{86}Sr)_{CHUR}=0.0827$, $(^{87}Sr/^{86}Sr)_{CHUR}=0.7045$, $(^{147}Sm/^{144}Nd)_{CHUR}=0.1967$ and $(^{143}Nd/^{144}Nd)_{CHUR}= 0.512638$. The depleted mantle model age (T_{DM}) was calculated using present–day $(^{147}Sm/^{144}Nd)_{DM}=0.2137$ and $(^{143}Nd/^{144}Nd)_{DM}=0.51315$.

4. Results

4.1. Mineral compositions

The chemical compositions of both silicate and oxide minerals from the Wajilitag and Puchang complexes, together with previously published data from the Wajilitag complex can be found in Supplementary Data Electronic Appendices 2–6.

The olivine in the Wajilitag clinopyroxenite and melagabbro has forsterite contents [Fo=molar Mg/(Mg+Fe)] ranging from 0.67 to 0.77 and from 0.67 to 0.75, respectively, with intra–sample variations commonly within 1 mol.% Fo content (Supplementary Data Electronic Appendix 2). Olivine in Wajilitag ores contains slightly higher Fo contents (0.76–0.80; Fig. 8a) and some individual olivine crystals in the ores exhibit reversed zoning marked by lower–Fo cores and higher–Fo rims. The clinopyroxene grains from the Wajilitag clinopyroxenites, melagabbros and disseminated ores have broadly similar Mg–number ($Mg^{\#}$=molar $Mg/(Mg+Fe^{2+}+Fe^{3+})$], ranging from 0.75 to 0.84, from 0.73 to 0.83 and from 0.73 to 0.80, respectively (Fig. 8b and c). Some zoned

clinopyroxene crystals in the clinopyroxenites and melagabbros display normal zoning (Supplementary Data Electronic Appendix 3), probably indicating the subsolidus equilibration between clinopyroxene and evolved magma during cooling (Li et al., 2012a). Plagioclase in Wajilitag clinopyroxenites has a relatively uniform composition with anorthite contents [An=molar Ca/(Ca+Na+K)] ranging from 0.71 to 0.76. Plagioclase in melagabbros have relatively lower An values (mostly between 0.44 and 0.65; Fig. 9a). Plagioclase in the disseminated ores shows wide compositional variations with An content ranging from 0.41 to 0.79 (Supplementary Data Electronic Appendix 4). Magnetite grains from the Wajilitag silicate rocks and disseminated ores show large ranges of Fe_2O_3 (32.6–63.9 wt.%), FeO (31.6–42.6 wt.%) and TiO_2 (1.44–17.9 wt.%) (Supplementary Data Electronic Appendix 5), which may be the result of subsolidus re–equilibration and exsolution during cooling. Particularly, magnetite grains in the disseminated ores tend to have higher Fe_2O_3, FeO, MgO and TiO_2 contents than those in the silicate rocks (Fig. 10a), a phenomenon also known in the Panzhihua and Hongge intrusions (Bai et al., 2012; Howarth et al., 2013; Pang et al., 2008b). Most magnetite inclusions hosted in the Wajilitag silicate minerals are commonly Cr–rich with 0.3 to 3.2 wt% Cr_2O_3 (Supplementary Data Electronic Appendix 6), higher than 'interstitial' magnetite grains present in above silicate rocks and disseminated ore (Fig. 10b). Except for a few samples, ilmenite grains in the Wajilitag disseminated ores also have higher TiO_2 and MgO contents than those in the barren silicate rocks (Fig. 10c). Ilmenite inclusions within the Wajilitag silicate minerals also tend to have lower TiO_2 and MgO contents than 'interstitial' ilmenite grains.

Compared to Wajilitag, olivine in Puchang barren leucocratic (i.e., gabbroic and anorthositic) rocks and disseminated ores contains lower Fo values (0.62–0.65 and 0.56–0.65, respectively). Olivines in Puchang massive ores have the highest Fo contents (0.75–0.76) (Fig. 8a and Supplementary Data Electronic Appendix 2). The Puchang olivine crystals are also relatively

lower in NiO contents than the Wajilitag olivine (Fig. 8a), although absolute NiO concentrations (≤0.2 wt.% and ≤0.08 wt.%, respectively) are low. Clinopyroxene from the Puchang barren leucocratic rocks and disseminated ores tends to have lower $Mg^{\#}$ values (0.69–0.76 and 0.70–0.76, respectively; Fig. 8b) and TiO_2 contents (Fig. 8c). Clinopyroxene grains of Puchang massive ores have high $Mg^{\#}$ values (0.74–0.76) compared to barren silicate rocks and disseminated ores. The clinopyroxene from the Puchang plagioclase–bearing clinopyroxenite exceptionally have the highest total alkalis (Na_2O+K_2O=0.50–1.0) and lowest $Mg^{\#}$ (0.44–0.61) and highest Na_2O (0.50–0.99) contents throughout the entire complex (Fig. 8b and Supplementary Data Electronic Appendix 3). No significant zoning is observed in individual clinopyroxene crystals in the Puchang complex. Clinopyroxene from the Puchang samples commonly have low Cr_2O_3 abundances relative to those of the Wajilitag (Fig. 8b). The An values of plagioclase in the Puchang gabbroic and anorthositic rocks spans a small range from 0.42 to 0.64, overlapping that of oxide ores (An=0.43–0.59) (Fig. 9b and Supplementary Data Electronic Appendix 4). Likewise, the 'intercumulus' magnetite crystals from the Puchang different types of ores and rocks also show large ranges of Fe_2O_3 (36.8–53.2 wt.%), FeO (35.4–41.0 wt.% and TiO_2 (5.54–13.5 wt.%) (Supplementary Data Electronic Appendix 5), but those in the ores (particularly the massive ores) always have higher Fe_2O_3, FeO, MgO and TiO_2 contents than those in the silicate rocks (Fig. 10a). Magnetite in the oxide inclusions hosted in olivine, clinopyroxene and plagioclase has similar amounts of MgO, TiO_2 and Cr_2O_3 to 'interstitial' magnetite grains in the samples (Fig. 10a, b). Except two samples, the majority of ilmenite grains in the disseminated and massive ores also have higher TiO_2 and MgO contents than those in the barren silicate rocks (Fig. 10c). Ilmenite inclusions hosted in the silicate minerals have somewhat lower MgO and TiO_2 contents than 'interstitial' ilmenite grains present in the Puchang gabbro samples.

4.2. Whole rock major and trace elements

The full data set of new and published major and trace element compositions from the Wajilitag and Puchang complexes is listed in Supplementary Data Electronic Appendix 7. For the Wajilitag clinopyroxenites and disseminated ores, CaO decrease whereas Al_2O_3, TiO_2, TFeO increase with decreasing MgO. For the melagabbro samples, SiO_2, Al_2O_3 and total alkalis increase, whereas CaO, TiO_2 and TFeO decrease with decreasing MgO (Fig. 11). It is noteworthy that the P_2O_5 contents in all studied samples from the Wajilitag complex are quite low, ranging from 0.01 to 0.79 wt.%. In the Puchang complex, a complicated variation that SiO_2, TFeO and Cr form near–horizontal trends and Al_2O_3, TiO_2, CaO and total alkalis exhibit slightly increasing trends when MgO contents decrease from ca. 18 wt.% to 8 wt.%, and then SiO_2, Al_2O_3, CaO and total alkalis increase continuously, whereas TFeO, TiO_2 and Cr significantly decrease with decreasing MgO for all barren gabbroic and anorthositic rocks. The Puchang clinopyroxenites have notably high CaO (20.8–22.2 wt.%) and low Al_2O_3 (7.1–9.3 wt.%) and total alkalis (0.85–1.2 wt.%) concentrations and plot in a tight cluster separately from the other samples (Fig. 11). The Puchang Fe–Ti oxide ores are characterized by a large range of TFeO (20.4–65.8 wt.%) and TiO_2 (3.5–13.7 wt.%) contents. Apart from clinopyroxenite samples (D8–1 and D8–3) having a slightly higher P_2O_5 content (0.58–2.2 wt.%), most of our studied samples from the Puchang complex also exhibit significantly low P_2O_5 concentrations (<0.1 wt.%).

For the Wajilitag complex, the clinopyroxenite and disseminated ores have similar but variable V, Ni and Cr concentrations, and the melagabbros have lower V (248–641 ppm), Ni (40.6–186 ppm) and Cr (15.1–177 ppm) contents. The absolute abundances of incompatible trace elements in the melagabbro samples except for two melagabbroic samples (ZK4503–1 and DW33–1) are significantly higher than both clinopyroxenites and disseminated ores (Fig. 12a, b). The Wajilitag samples display parallel and slightly fractionated

chondrite–normalized rare earth element (REE) patterns with general enrichments in light REEs relative to heavy REEs [$(La/Yb)_N$=3.0–22.8, Subscript *N* denotes the chondrite–normalized] (Fig. 12e, f). Apart from two gabbroic sample (ZK4503–1 and DW33–1) with Eu/Eu* ratios of 1.08 and 1.48, most silicate rocks and Fe–Ti oxide ores from the Wajilitag complex lack any significant Eu anomalies (Eu/Eu*=0.91–1.05; Fig. 12e, f).

For the Puchang complex, vanadium and nickel abundances range from 113 to 985 ppm and 10.5 to 23.7 ppm in the silicate rocks, respectively, to ~100 ppm or higher in the Fe–Ti oxide ores. The Puchang gabbroic and anorthositic rocks have similar light REE–enriched chondrite–normalized patterns [$(La/Yb)_N$=1.2–12.9], with the relatively low total REE concentrations observed in the anorthosites (Fig. 12g, h). All gabbroic and anorthositic samples show obvious and variable positive Eu anomalies (Eu/Eu*=1.02–3.43; Fig. 12g). The Puchang oxide ore samples have the lowest total REE abundances and nearly flat chondrite–normalized REE patterns [most $(La/Yb)_N$<6; Fig. 12h] with positive or negative Eu anomalies (Eu/Eu*=0.71–1.67). The most striking characteristic is that the concentrations of incompatible trace elements in the Puchang clinopyroxenites are about one order of magnitude higher than in the other rocks (Fig. 12c, d).

4.3. Sr–Nd isotopes

Representative Sr and Nd isotopic compositions in 5 clinopyroxene separates and 25 whole–rock samples are reported in Table 2 and the full data set of new and previous Sr–Nd isotope compositions are presented in Supplementary Data Electronic Appendix 8.

All samples from various parts of the Wajilitag complex are characterized by a small range of initial $^{87}Sr/^{86}Sr$ ratios (I_{Sr}) from 0.7038 to 0.7048 and positive age–corrected ε_{Nd}(t=283 Ma) values varying from 0.04 to 3.01. As illustrated in Fig. 13, the isotopic compositions obtained in this study are similar to or slightly more limited than those previously published by Cao et al. (2014).

In Puchang, one plagioclase–bearing clinopyroxenite sample (D61–2), was collected in the most external part of the contact zone, with significantly high initial $^{87}Sr/^{86}Sr$ ratios (0.7078) and low $\varepsilon_{Nd}(t)$ value (–1.67). The other barren samples have I_{Sr} ranging from 0.7039 to 0.7059 and age–corrected ε_{Nd}(t=275 Ma) values ranging from –1.05 to 2.35, with the highest $\varepsilon_{Nd}(t)$ values observed in one plagioclase–bearing clinopyroxenite sample (D8–3) from the contact zone. The oxide ore samples in the Puchang complex show relatively uniform I_{Sr} ranging from 0.7045 to 0.7058, and near–zero $\varepsilon_{Nd}(t)$ values ranging from –0.16 to 0.02. Although the compositions broadly overlap, the Wajilitag samples have slightly lower I_{Sr} and higher $\varepsilon_{Nd}(t)$ values than the Puchang samples (Fig. 13). As a whole, the Wajilitag and Puchang data partially overlap with or are close to the field of the kimberlitic rocks, which also occurred in the study area, whereas almost all samples from both complexes display distinctively lower I_{Sr} and higher $\varepsilon_{Nd}(t)$ values in comparison with the Tarim basalts (Fig. 13).

5. Discussion

5.1. Crystallization sequences

The petrography of the Wajilitag clinopyroxenite suggests that olivine and clinopyroxene are cumulus phases, whereas the Fe–Ti oxides (magnetite and ilmenite) and plagioclase are interstitial between olivine and clinopyroxene. This implies later crystallization of plagioclase and Fe–Ti oxides compared with cumulus olivine and clinopyroxene. In addition, smaller Fe–Ti oxide grains occur as inclusions in some clinopyroxene grains, indicating that they crystallized simultaneously. The higher Fo contents of the olivine and $Mg^{\#}$ contents of the clinopyroxene in the Wajilitag clinopyroxenite samples relative to the Wajilitag melagabbros also suggest that olivine and clinopyroxene have crystallized before Fe-Ti oxides and plagioclase.

Cumulus plagioclase and olivine grains in the Puchang massive ores are

commonly corroded and reacted, and have distinct reaction rims, suggesting that a considerable amount of silicate grains may represent early crystallized silicate phases (prior to the Fe–Ti oxides). The rock textures in the Puchang complex suggest that the possible order of crystallization in the Puchang complex is olivine and clinopyroxene, followed by plagioclase, and then Fe-Ti oxides. The relatively lower An contents of the plagioclase in the Puchang ore samples relative to the Puchang barren silicate rocks (Figs. 9) also suggest that plagioclase has crystallized before Fe-Ti oxides. It would be worth mentioning that Wajilitag contains the most primitive mineral assemblage with olivine + clinopyroxene. This primitive stage of evolution is absent in Puchang.

The contrast in the Fo contents of olivines and $Mg^{\#}$ values of clinopyroxenes between the barren silicate rocks and massive oxide ores in the Puchang complex (Figs. 8a, b) probably reflects subsolidus Fe–Mg exchange reaction between oxides and silicates during cooling and causing Fe–Ti oxides to become richer in Fe, and ferromagnesian minerals richer in Mg in samples containing abundant Fe–Ti oxides (Pang et al., 2009; Shellnutt and Pang, 2012). Confidence in this inference is reinforced by commonly reversely zoned with higher Mg rims in individual olivine crystals in the ores. In comparison, the lack of strongly Mg enrichment in olivine and clinopyroxene present in the disseminated ores from the Wajilitag and Puchang complexes, may suggest the influence of such a subsolidus re–equilibration process has not been very significant or is probably related to concurrent exsolution of Fe–Ti oxides, as evident from textural observations, during re–equilibration (Bai et al., 2012).

5.2. Parental magma compositions

The Puchang marginal rocks (e.g., the plagioclase–bearing clinopyroxenites) have moderate MgO contents and distinctly high P_2O_5 concentrations, combined with the highest concentration of incompatible elements, indicating that the clinopyroxenites were crystallized from highly

differentiated magma (Figs. 11 and 12). Clinopyroxene grains in the samples with low MgO and high TFeO contents (Fig. 8b) have straight boundaries and meet at triple junctions (Fig. 6f) clearly indicating significant recrystallization after their formation (Howarth and Prevec, 2013b). We thus tentatively propose that the plagioclase–bearing clinopyroxenite samples of the marginal zone may represent samples of evolved fractionates of the parental magma and not of this magma itself. Furthermore, obvious marginal chilled rocks that could be representative of liquid compositions are not found and there is clear evidence of crystal accumulation in the Wajilitag complex. Thus, the parental magma compositions of the Wajilitag and Puchang complexes are difficult to estimate. The presence of abundant Fe–Ti oxide inclusions in cumulus olivine and clinopyroxene (Figs. 4–7) suggest Fe–Ti–rich parental magmas.

An approach proposed by Roeder and Emslie (1970) could be employed to further constrain the potential parental (not primary) magma composition of the complexes. Based on the well–established olivine–melt Mg–Fe distribution coefficient $K_D=(FeO/MgO)^{olivine}/(FeO/MgO)^{liquid}$ of 0.3±0.03, a commonly observed value in experimental systems and natural rocks (Falloon and Danyushevsky, 2000), and the composition of the most magnesian olivine from the Wajilitag and Puchang intrusive rocks (Fo=0.77 and 0.65, respectively, found as middle grains in the Wajilitag clinopyroxenite and Puchang gabbro), we obtain that the melts in equilibrium with these cumulus olivine grains in these complexes had the $Mg^{\#}$ of between 0.45 and 0.55, and between 0.32 and 0.39, respectively.

Such $Mg^{\#}$s are much lower than for the primary magmas derived from the mantle, which generally have high $Mg^{\#}$ (around 0.7 or more; Frey et al., 1978; Wilson, 1989), implying that the parental magmas most probably represent the evolved basaltic magmas resulting from a previous process of fractionation of the more primitive magmas before entering the complexes. The cumulus assemblage in the early–formed rocks of the Wajilitag and Puchang complexes comprises olivine+clinopyroxene/plagioclase+Fe–Ti oxides, suggesting that

the magmas experienced evolution prior to their final emplacement. Compared with the mantle–derived olivine (Fo>0.85; Roeder and Emslie, 1970; Zhang et al., 2006), the relatively low Fo contents (0.51–0.80) in both complexes also indicate that the parental magmas have experienced moderately fractional crystallization before they entered the complexes. The relatively low Ni contents of olivine and low total PGE abundances and high Pd/Ir ratios (up to 53) in Wajilitag and Puchang, are additionally a signature of differentiated magmas (Zhang et al., 2014).

The above calculated minimum $Mg^{\#}$ of the Wajilitag parental magma is higher than that of the Puchang, implying that the former may have been less evolved than that of the latter before entering the complexes, although they belonged to the same kindred. Cumulus olivine and clinopyroxene in the Wajilitag complex have high Fo or $Mg^{\#}$, NiO and Cr_2O_3 contents relative to those in the Puchang complex (Figs. 8a, b and 12), also demonstrating that the Wajilitag parental magma may have been considerably more primitive than that of the Puchang. Furthermore, the clinopyroxene grains from Wajilitag clinopyroxenites, melagabbros and disseminated ores have relatively higher TiO_2 contents than those from the Puchang gabbroic and anorthositic rocks and disseminated ores (Fig. 8c), implying that the parental magma for the Wajilitag deposit also has higher TiO_2 content than that for the Puchang deposit. The Wajilitag rocks have lower Fe^{3+}/Ti^{4+} ratios than the Puchang rocks (Fig. 11h), further demonstrate that the Wajilitag parental magma had higher TiO_2 contents than that of the Puchang complex, because the crystallization of ilmenite is mainly controlled by the TiO_2 content in magma (Charlier et al., 2006).

Recently, Zhang et al. (2008) and Cao et al. (2014) have suggested that the high–Mg mafic dyke sample W13 in this region reported by Jiang et al. (2004b) can be regarded as the parental magma of the Wajilitag mafic–ultramafic rocks. The sample having 13.6 wt.% TFeO, 2.9 wt.% TiO_2 and 8.9 wt.% MgO and $Mg^{\#}$ of 0.54 (Table 3) is also consistent with the

parental magma composition predicted by the most Mg–rich olivine in the complex using olivine–liquid equilibrium. Similarly, the least fractionated mafic dyke sample (ZK4–2–15–3, Table 3) associated with the Puchang complex could be plausible candidate for the parental magma for the complex. The sample contains 14.0 wt.% TFeO, 2.7 wt.% TiO_2 and 4.6 wt.% MgO and $Mg^{\#}$ of 0.37, which is comparable with the above estimated compositions of parental magma of the complex. Therefore, the estimated Wajilitag parental magma may contain slightly higher MgO and TiO_2 contents than that of the Puchang complex, although both parental magmas show slightly fractionated REE patterns (Fig. 12), which may be derived from various differentiation of more primitive melts at depth. The data compiled in Table 3 clearly indicated that the TFeO and TiO_2 contents of Wajilitag and Puchang parental magmas are much higher than those of some classical ferrobasaltic intrusions in the world, including the Skaergaard, Panzhihua and Taihe intrusions. In detail, The Wajilitag parental magma is relatively close in composition to that of the Hongge ore–bearing intrusion in the ELIP (Bai et al., 2012), but slightly lower in TFeO and TiO_2 contents. The Puchang parental magma is compositionally overall similar to that of the Sept Iles ore–bearing intrusion (Namur et al., 2010).

5.3. Early magnetite saturation in Wajilitag

It seems that the Wajilitag and Puchang complexes experienced somewhat different fractionation processes, and one of the most striking differences is that most Fe–Ti oxides reached the liquidus probably after the appearance of mafic silicate minerals but at the same time as the appearance of plagioclase in the Wajilitag complex, whereas most Fe–Ti oxide minerals join the liquidus after plagioclase in the Puchang complex. The relatively higher Cr_2O_3 and NiO contents of the oxide inclusions and Fo or $Mg^{\#}$ values of the oxide inclusion–bearing olivine and clinopyroxene crystals at Wajilitag (Figs. 8 and 10b), further indicating that crystallization of magnetite at Wajilitag

was relatively earlier than that at Puchang during magma differentiation. This inference is in accordance with our field observation that Fe–Ti oxide mineralization in the Wajilitag complex is concentrated in the clinopyroxenite portions, whereas both massive to disseminated Fe–Ti oxide ores in the Puchang complex mainly within the gabbroic section. Indeed, compared with some well–studied oxide ore–bearing intrusions in the world, the silicate phases in the Wajilitag complex are relatively primitive at the onset of Fe–Ti saturation (Table 4; Namur et al., 2010; Pang et al., 2009; Tegner et al., 2006).

Melting experiments (Botcharnikov et al., 2008; Juster et al., 1989; Toplis and Carroll, 1995) and geochemical studies (Namur et al., 2010; Pang et al., 2008b) have indicated that the parameters controlling the relative timing of the arrival of Fe–Ti oxides on the magmatic systems include (1) the composition of the parental magma, in particular the TFeO and TiO_2 contents, (2) the fO_2 conditions, and (3) the presence of volatiles. There is a consensus that the different sequences of crystallization in ferrobasaltic magmas are related to the composition of the starting material (Namur et al., 2010 and references therein). As stated below, the parental magmas of the two complexes originated from metasomatized mantle sources were already rich in Fe and Ti. Pervious studies also suggested that the FeO– and TiO_2–rich magma would offer more chance to develop Fe–Ti oxides than normal basaltic magma (Bai et al., 2012; Song et al., 2013; Toplis and Carroll, 1995). As the enrichment in TFeO and TiO_2 contents in the Wajilitag parental magma is highly significant compared with other classical Fe–Ti oxide ore–bearing intrusions (Table 3), it is to be expected that Fe–Ti oxide minerals crystallized in the Wajilitag magmatic system relatively early as compared to the Puchang magmatic system. That is, the compositional characteristics of the parental magmas could be postulated as an important factor controlling the relative order of crystallization between Fe–Ti oxides and silicate minerals (in particular plagioclase), in perfect agreement with the conclusions drawn from previous experimental and mineralogical studies (Bai et al., 2012; Namur et al., 2010;

Snyder et al., 1993; Toplis and Carroll, 1995).

Crystallization experiments in ferrobasaltic systems indicated that the time of Fe–Ti oxide saturation and crystallization in magmatic systems are largely controlled by fO_2 (Berndt et al., 2005; Botcharnikov et al., 2008; Juster et al., 1989). This observation to some extent led many researchers (Bai et al., 2012; Ganino et al., 2008) to propose that the crystallization of Fe–Ti oxides at relatively primitive stages in some magmatic systems (e.g., Panzhihua and Hongge) was caused by high oxidation states as a result of small amount (e.g., 8–13%) assimilation of the carbonate wall rocks. However, the country rocks of the Wajilitag complex are terrestrial clastic rocks. Furthermore, Toplis and Carroll (1995) have stressed that magnetite–dominated oxide assemblages crystallize at high oxidation states (fO_2=FMQ+1.5), whereas those containing cumulus magnetite and ilmenite crystallize at fO_2 at FMQ. The fact that some oxide inclusions in the Wajilitag samples contain coexisting titanomagnetite and ilmenite cumulus phases, therefore indicate that these inclusions crystallized at relatively low oxidized conditions, likely close to FMQ+1. The common occurrence of sulfides and ilmenite lamellae intersecting at 60° and 120°interfacial angles with magnetite in the Wajilitag ore–bearing rocks again imply the low fO_2 at magmatic temperatures, since sulfides are stable only at the oxidation state below FMQ+1.5 in various magmatic systems (Howarth et al., 2013; Jugo, 2005).

As an alternative to the high fO_2 of the magmas involved, the presence of water in basaltic magma systems could have lowered the liquidus temperature of silicate phases (mainly plagioclase), but tends to a limited effect on oxide minerals (Berndt et al., 2005; Botcharnikov et al., 2008; Howarth et al., 2013). These experimental studies indicated that the elevated H_2O contents can result in crystallization of clinopyroxene and Fe–Ti oxides before plagioclase, and therefore the relatively early arrival of Fe–Ti oxides in the magmatic systems. The hypothesis is reconciled with the sequence of liquidus phase appearance at the Wajilitag. As noted in a previous section, the low proportion

of cumulus plagioclase in the Wajilitag intrusive rocks may also favour a parental magma with relatively high H_2O content in order to depress the plagioclase crystallization temperature sufficiently so that only some ferromagnesian minerals and Fe–Ti oxides crystallize from the magma.

To sum up, the early saturation of Fe–Ti oxides in the Wajilitag complex is probably due to a combination of more primitive Fe–Ti–rich parental magma and rather high initial H_2O content.

5.4. Evolution of liquid compositions

In order to better understand the sequence of crystallization and the evolutionary trend of the Wajilitag and Puchang ferrobasaltic magmas, the PELE version of the MELTS algorithm (Boudreau, 1999) was applied to model the ferrobasaltic liquid line of descent and mineral–melt equilibrium. As described above, two most primitive crosscutting dyke samples W13 and ZK4–2–15–3 can be best candidates for the parental magmas of the Wajilitag and Puchang complexes, respectively. Experimental investigations by Berndt et al. (2005) and Botcharnikov et al. (2008) demonstrated that the crystallization sequence of silicate minerals (in particular plagioclase) is significantly affected by the H_2O content of the parent magma. High H_2O contents of magma can result in significantly lower crystallization temperatures for plagioclase. The low contents of cumulate plagioclase in the Wajilitag complex suggest that the Wajilitag parental magma contained much more initial H_2O content than the Puchang complex. Considering that the Wajilitag and Puchang complexes do not contain primary hydrous minerals (e.g., amphibole) in the early cumulate rocks, also suggesting that the parental magmas could not contain considerable amounts (e.g., >2 wt.%) of water, because some experimental investigations have indicated that crystallization of hornblende needs 2–5 wt.% H_2O in the magma (Botcharnikov et al., 2008; Howarth and Prevec, 2013a). Evidence presented here indicates that the Wajilitag parental magma crystallized at relatively high initial water content,

likely 2.0 wt.%, whereas the initial water content of the Puchang parental magma was more likely close to 1.0 wt.%.

Some experimental investigations showed that the crystallization of Fe–Ti oxides from ferrobasaltic magma is mainly controlled by higher oxidation states (>FMQ, FMQ=fayalite–magnetite–quartz buffer; Toplis and Carroll, 1995). Notably, coexistence of sulfides with Fe–Ti oxides in the Wajilitag and Puchang complexes may indicate that the oxidation state at magmatic temperatures was no more than FMQ+2 (Jugo, 2005). Thus, it is reasonably expected that the fO_2 was set using the oxygen buffer FMQ+1. Similar values have been obtained for the Panzhihua and Hongge intrusions of the ELIP (Bai et al., 2014). The pressure is difficult to constrain, because we cannot know the exact depth of their final emplacement. Indeed, some studies also showed that the pressure of crystallization does not significantly affect the crystallization sequence (Howarth and Prevec, 2013a). As the typical range of pressure observed in the most ore–bearing intrusions is close to 1 kbar, the pressure was set at 1 kbar in this study to constrain the effect of pressure on the crystallization sequence of these basaltic magmas. Temperature increments were set at 10 °C for an isobaric system undergoing fractionation. The parent magma compositions were renormalized to 100 wt.% to accommodate for the variable amounts of H_2O added to the composition. Modeling runs ran to 65–70% crystallization of the parent magmas. Results are listed in Supplementary Data Electronic Appendix 9. As shown in Fig. 14, olivine is the first phase to appear on the liquids (1190 °C), followed by clinopyroxene (1070 °C) in the Wajilitag chamber. The modeled compositions of olivine (Fo=0.68–0.84) and clinopyroxene ($Mg^{\#}$=0.79–0.82) are broadly consistent with the electron microprobe data of olivine (Fo=0.67–0.80) and clinopyroxene ($Mg^{\#}$=0.75–0.84) of the Wajilitag clinopyroxenites. Magnetite mainly crystallizes together with plagioclase at 1020 °C after fractional crystallization of ~10.5% olivine and ~6.9% clinopyroxene (Supplementary Data Electronic Appendix 9). In the Puchang magma chamber, plagioclase crystallizes from

the more evolved magma at 1110 °C followed by olivine when temperature decreases to 1100 °C. Clinopyroxene and magnetite are the liquidus phases after fractional crystallization of ~17.7% plagioclase and ~6.7% olivine (Supplementary Data Electronic Appendix 9). The calculated compositions of plagioclase (An=0.42–0.69), olivine (Fo=0.60–0.72) and clinopyroxene ($Mg^{\#}$=0.75–0.76) are roughly compared with the range of mineral compositions observed in the Puchang complex (An=0.42–0.64, Fo=0.62–0.65 and Mg#=0.69–0.76, respectively).

5.5. Origin of ferrobasalt parental magmas

To evaluate the mantle source characteristics of the Wajilitag and Puchang complexes, it is necessary to first unravel the extent of crustal contamination, because crustal contamination is a common process during ascent or solidification of mantle-derived melts within continental crust. Indeed, the xenoliths of the country rocks within the contact zone of the Puchang complex and the notably high I_{Sr} and low $\varepsilon_{Nd}(t)$ value of the sample (D61–2) from the most external part of the zone (Fig. 13), clearly imply that the magma was contaminated by the wall rocks (e.g., carbonates) *in situ*. However, the other plagioclase–bearing clinopyroxenite sample (D8-3) a short distance away from the immediate contact has the highest $\varepsilon_{Nd}(t)$ and moderately low I_{Sr} values among the studied samples from the Puchang complex, which cannot be simply explained by extensive crustal assimilation as it expected to markedly change the Sr–Nd isotopic compositions throughout the complex, for the contact zone in particular (DePaolo, 1981). Moreover, the Wajilitag and Puchang samples (with the exception of sample D61–2) independently show little Sr–Nd isotopic variation (Fig. 13), also confirmed the above inference. The mantle xenolith sample (W10–97; Jiang et al., 2004a) entrained within the kimberlitic rocks in northwestern Tarim Craton can be considered to be the primary source. If the compositions of the early–middle Paleozoic carbonate rocks from the northern Tarim Craton are taken as the crustal contaminant, the

modeling results suggest significantly high amounts of bulk–crustal contamination (mostly 20–50%) were ingested into the primary melt parental to these intrusive rocks (Fig. 13). However, the important observation that the $\delta^{18}O$ composition of the zircons from the various lithologic units of the complexes is closed to typical mantle zircon values (Zhang et al., 2016), does not support the model of such high degree of carbonate contamination for the primary magmas, because carbonate assimilation should affect the O–isotope composition of the contaminated magma and any minerals crystallized from it (Pang et al., 2015). Moreover, both Tarim lower and upper continental crustal materials (e.g., Neoproterozoic gabbros and granites, and early–middle Paleozoic granites) as the basement through which the magmas passed, simple mixing calculations based on their Nd–Sr isotope compositions show that the studied intrusive rocks (again except for sample D61–2) contain no more than 10% of crustal components (Fig. 13). Combining the above arguments, crustal contamination or assimilation must have played a role in the petrogenesis of the intrusive rocks, particularly in the contact zone and ore bodies of the Puchang complex, but the effect is insignificant in explaining the isotope geochemical features in these rocks. Instead, the isotopic compositions of most samples from the main body of the complexes should reflect the composition of their mantle sources.

It is widely recognized that the Fe–Ti oxide ore–bearing intrusions in the ELIP with the present–day Ocean Island Basalts (OIB)–like signatures appear to have been derived from a slightly enriched asthenospheric melt (Bai et al., 2012; Zhang et al., 2009). However, it must be noted that the broadly OIB–like characteristics are not persuasive evidence for a source originating from a convective asthenospheric mantle, as the interaction between a depleted non–convecting lithospheric mantle source and invading a late metasomatic (enriching) component would also have given an OIB–like isotopic signature to some mafic–ultramafic rocks (Zhang et al., 2013 and references therein). Fortunately, the available kimberlitic rocks and their hosted mantle xenoliths

(e.g., dunite and pyroxenite xenoliths) in the northwestern TLIP may represent exhumed fragments of the subcontinental lithospheric mantle (SCLM; Zhang et al., 2013). The Wajilitag and Puchang samples display a coherent Sr–Nd isotopic trend with the kimberlitic rocks, which were interpreted to be derived from a lithospheric mantle source modified by ancient subduction materials (Zhang et al., 2013). Note that both the complexes and kimberlitic intrusions showed close proximity and a nearly coeval nature, thus the basaltic parental magmas were most plausibly derived from enriched lithospheric mantle, rather than the convective asthenosphere or a deep mantle plume.

Previous studies suggested that the northern margin of the Tarim Craton, where the Wajilitag and Puchang complexes are located, has undergone two periods of oceanic lithosphere subduction, which occurred in the Neoproterozoic and early–middle Paleozoic times, respectively. It is generally accepted that long–term isolation of a metasomatized mantle lithospheric domain, which has very high contents of Th, U, Rb, Sr and light REE, would facilitate in–growth of an enriched Sr–Nd isotopic signature (Thompson and Gibson, 1994). As a corollary, the Proterozoic subduction processes could not account for the well–defined Sr and Nd isotope signatures of the intrusive rocks, which are depleted relative to present–day Bulk Earth, and perhaps the most plausible explanation is that the lithospheric mantle beneath the northern part of the Tarim Craton has been previously metasomatized by slab–derived fluid/melt during early–middle Paleozoic subduction. The oceanic subduction and metasomatic events affecting the ancient lithospheric mantle during the early–middle Paleozoic in the Tarim Craton have also been confirmed in previous studies (Zhang et al., 2013 and references therein). The minor Sr–Nd isotopic differences between the two igneous complexes (Fig. 13) may be suggested that their mantle sources could be slightly heterogeneous.

Qu et al. (2011) suggested that the early–middle Paleozoic subducted oceanic slab probably likely underwent dehydrated eclogite facies metamorphism and generated slab melts, a scenario supported by the

presence of the ca. 430 Ma diorites with residual amphibolite and eclogite in the source within the Baicheng area, which is not far from the study area (Zhao et al., 2015). Indeed, the upward migration of slab–derived fluids/melts into the overlying ambient lithospheric mantle could lead to the formation of metasomes (e.g., pyroxene, phlogopite and/or amphibole; Tuff et al., 2005). Further partial melting of the residual eclogite could also produce highly siliceous andesitic melts that likely ascended and reacted with surrounding ambient peridotitic mantle through which they percolate, producing hybrid garnet and pyroxene lithologies (Yaxley and Sobolev, 2007), forming the equivalent of low–silica eclogite or garnet pyroxenite in the lithospheric mantle. This scenario is supported by the presence of peridotite, clinopyroxenite and amphibolite mantle–derived xenoliths as well as phlogopite, garnet and clinopyroxene entrained xenocrysts in the Wajilitag kimberlitic rocks (Zhang et al., 2013). Experimental and geochemical studies have revealed that the formation of Phanerozoic primitive Fe–rich magmas is genetically related to the presence of eclogite or garnet pyroxenite in the source under high pressure (~5 GPa) and temperature (~1550 °C) (Tuff et al., 2005; Yaxley, 2000). Hence, the Wajilitag and Puchang ferrobasalt parental magmas can be generated by partial melting of the enriched subcratonic lithosphere mantle that has incorporated subduction-related components.

Importantly, the major contribution of the Tarim mantle plume might only provide the heat to trigger partial melting of the metasomatized SCLM. It is reasonably safe to conclude that the recycled subduction–related materials (including subsequent reaction products, i.e., eclogite and garnet pyroxenite) preserved within the lithospheric mantle are a critical source for the generation of these ferrobasalt magmas. Actually, recent studies have shown that melts derived from pyroxenite relative to peridotite sources are characterized by lower CaO/MgO and high FeO/MnO ratios (> 60; Howarth and Harris, 2017 and references therein). The ferrobasaltic parental magmas with low CaO content relative to MgO and high FeO/MnO ratios (73-90; Table 4) are also

consistent with a pyroxenite dominated mantle source. Confirmation of our view also comes from some experimental studies (Tuff et al., 2005; Yaxley, 2000 and references therein), which have demonstrated that melting of garnet pyroxenite under high pressure (e.g., ~5 GPa) and temperature (e.g., ~1550 °C) is necessary for generating Fe–rich magmas.

5.6. Implications for the formation of Fe–Ti oxide deposits

Although the Fe–Ti oxide ores are frequently associated with mafic–ultramafic intrusive rocks, the processes leading to concentration of Fe–Ti oxide ores from magmas is not well understood. The main controversy concerning the origin of the Fe–Ti oxide ores is whether they are differentiated cumulates formed by crystal fractionation from Fe– and Ti–rich magmas by density–driven crystal settling and sorting of minerals, or they crystallize from an Fe–Ti–rich silicate melt segregated from its Si–rich immiscible conjugate.

It has been recognized that oxide–silicate liquid immiscibility developed during the late–stage differentiation of the Fe–rich magmas in nature and in the laboratory (Charlier and Grove, 2012). Many previous experiments have shown that elevation of phosphorus contents promotes the development of two immiscible liquids and the hypothetical Fe–rich immiscible liquid commonly showed strong enrichment in P_2O_5, REE and HFSEs (Charlier and Grove, 2012). In such case, many magmatic Fe–Ti oxide ores contain abundant apatite (~30%), for example, nelsonites in anorthosite complexes or mafic–ultramafic intrusions (Charlier et al., 2011; VanTongeren and Mathez, 2012). The Fo and Mg numbers of silicate minerals and the $Mg^{\#}$ of the proposed parental magma compositions in the Wajilitag and even Puchang complexes suggest that their parental magmas are not highly evolved and are much more primitive than those of the Skaergaard intrusion (Table 3). Additionally, Fe-Ti ores in the Wajilitag and Puchang complexes are not associated with apatite. Importantly, some peripheral evidence for separation of Fe– and Si–rich liquids is commonly identified from immiscible glass

droplets in the groundmass of basalts or distinct melt inclusions in silicates and apatite from plutonic rocks at the microscale (Charlier et al., 2011; Fischer et al., 2016; Liu et al., 2014; Veksler et al., 2007) which are absent in Wajilitag and Puchang. Thus, the formation of the Wajilitag and Puchang oxide deposits cannot be ascribed directly to the existence of an immiscible Fe–rich magma, and alternative mechanisms involving crystal fractionation with sinking and sorting of dense Fe–Ti oxide crystals must be invoked.

Massive Fe–Ti oxide ores are more common in the Puchang complex. This intrusion provides an excellent case study to identify the dominant process in the formation of the massive ores in ferrobasaltic magmas. The formation of the massive oxide ores in the Panzhihua and Hongge intrusions is that they resulted from the early crystallization and extensive accumulation of Fe–Ti oxides under oxidizing conditions due to an interaction of the basaltic magma with CO_2 degassed from sedimentary wall rocks, e.g., carbonate rocks Ganino et al., 2008). The wall rocks of the Puchang complex are composed of calcareous slate and marble. If magma and surrounding carbonate country–rocks interaction is the key to trigger ore formation, it might reasonably be expected to produce Fe–Ti oxides concentration at the magma–footwall contact zone (e.g., the immediate base of the complex). This is not observed to be the Puchang case. Additionally, the lack of significant break between the zircon O isotopic compositions of the Puchang intrusive rocks and established mantle zircon values (Zhang et al., 2016), suggests that the effect of contamination by sedimentary wall rocks resulting in the elevation of oxygen fugacity and to the subsequent formation of the massive oxide ores, is insignificant.

Instead, the cumulate texture of the silicate rocks and depletion of incompatible trace elements in the oxide ores and associated rocks in the Puchang complex as compared to the estimated parental magma would indicate significant loss of residual liquid in the samples. The low proportion of residual liquid left at the Puchang complex indicates that the complex has

probably recorded more evolved crystallization stages than Wajilitag complex. Besides, extensive gabbroic rocks within the Puchang complex, also imply a prolonged period of fractional crystallization before the appearance of cumulus Fe–Ti oxides that resulted in the concentration of large amounts of Fe and Ti in the residual magma. In this way, the residual magma becomes strongly enriched in the TFeO and TiO_2 and depleted in SiO_2 (Fig. 14 and Supplementary Data Electronic Appendix 9), which may promote subsequently extensive Fe–Ti oxide crystallization. As the above petrological model results, the percentage of crystallized Fe–Ti oxides before the saturation of apatite from the Puchang residual magma are probably up to 11, which is much higher than that of the Wajilitag (6.9 wt.%), likely resulting in the precipitation of relatively large amounts of Fe–Ti oxides required for the development of the massive oxide ores in the Puchang.

The relatively high proportion of the interstitial hornblende in the Puchang oxide ores indicated that the pre–existing residual magma when Fe–Ti oxides crystallized contained much more H_2O content than the Wajilitag complex (Fig. 6j and k). However, the above inference indicates that the Wajilitag parental magma contained more initial H_2O content than the Puchang complex. Thus, it is hard for a significantly increase in water content of the Puchang residual melt only via crystallization of anhydrous assemblages. Given the current evidence, it is likely that external water was introduced into the Puchang shallow magma chamber within the current emplacement site, more likely when the magma experienced extensive crystallization of Fe–Ti oxides. Ganino et al. (2008) documented that wet country rocks (such as carbonates) may represent a possible crustal source for the addition of H_2O for the Panzhihua magma system. Considering that the Puchang complex was directly intruded into the carbonate and experienced a long differentiation process, a potential source for the addition of H_2O for the Puchang magma system may be from the country rocks, because the residual magma could heat strata around the magma chamber and absorb the H_2O within it. Later

addition of water to the initially dry (~1 wt.% H_2O) magma during the crystallization of Fe–Ti oxides should significantly affect the crystallization temperature of silicates (in particular plagioclase) and resultantly consumed previously crystallized silicate grains (Howarth and Prevec, 2013a). The hypothesis could also be reconciled with the silicate disequilibrium textures observed in this study. Furthermore, previous studies suggested that the external water does not interact with the magma, but would induce Fe–Ti oxide saturation at the expense of plagioclase (Howarth and Prevec, 2013a; Howarth et al., 2013). The process could also effectively facilitate rapid transport and accumulation of the Fe–Ti oxides in the H_2O–enriched interstitial liquid. Meanwhile, later gravitational instability and rapid collapse of a portion of abundant Fe–Ti oxide cumulates, due to the density contrast ($\rho_{Fe–Ti\ oxides}$≥4.7 g/cm^3, $\rho_{plagioclase\ (An50)}$=~2.65 g/cm^3 and ρ_{cpx}=~3.5 g/cm^3) could also result in highly dense crystal slurries through hydraulic fractures. The large range of anorthite contents in the anorthositic samples (Fig. 9b) can be explained by redistribution of cumulus minerals, possibly by magma convection.

Considering that the Puchang intrusive rocks are mostly cumulates, the originally Fe–Ti oxide–rich slurries could further rapidly percolate downward through the underlying partially–solidified silicate crystal pile from higher up in the chamber and emplace to their current location and then form high–grade Fe–Ti oxide ore bodies, because such highly Fe–Ti oxide slurries would denser than the silicate crystal mush at a given level. Indeed, compared to the Wajilitag, the main Fe–Ti oxide ore bodies in Puchang generally show clear intrusive boundaries with the previously crystallized barren silicate rocks also suggesting that the ore bodies likely formed not *in situ*. The compaction of the crystal mush by effectively gravitational sinking and resorting of the Fe–Ti oxides could expel evolved intercumulus residual liquid out of the crystal matrix. A similar dense crystal slurry model has also been proposed for the emplacement of Fe–Ti oxide ore bodies and chromitite ore bodies within mafic–ultramafic intrusions (Eales and Costin, 2012; Howarth and Prevec,

2013a). In summary, it is reasonable to infer that the combined effect of protracted differentiation history of a highly Fe enriched parental magma and later addition of water to the magma after its final emplacement is required for the development of massive oxide ores in the present case.

Overall, the compiled data presented in the study may be used to propose several petrogenetic processes for the formation of the Wajilitag and Puchang complexes, which ultimately led to the formation of Fe–Ti oxide ores (Fig. 15).

(1) The Puchang and Wajilitag parental ferrobasaltic magmas derived from the enriched lithosphere mantle sources ascended into the Devonian clastic and Carboniferous carbonate strata, respectively (Fig. 15a, d). Different from the Puchang magma, early saturation of Fe–Ti oxides in the Wajilitag magma may be induced by more primitive Fe–Ti–rich parental magma and relatively high initial H_2O content.

(2) The Wajilitag and Puchang complexes experienced different crystallization path. Early and extensive crystallization of plagioclase, olivine with minor clinopyroxene from Puchang parental magma, and fractional crystallization of olivine and clinopyroxene with minor Fe–Ti oxides from Wajilitag parental magma formed the cumulate rocks (e.g., the Puchang gabbro and Wajilitag clinopyroxenite) (Fig. 15b, e). Continuous crystallization of these silicate minerals (in particular plagioclase in the Puchang magma system) then resulted in more Fe–rich residual melts. Because large amounts of the low density plagioclase joins the liquidus before Fe–Ti oxides in the Puchang magma chamber, the substantial amount of plagioclase crystals could rapidly transport and float upward to the upper part of the Puchang magma chamber, and subsequently form the anorthositic cumulates (Fig. 15b), in agreement with the widespread planar foliation and lineation shown by the orientation of plagioclase in some gabbro samples (Fig. 5i) and many anorthositic autolithic blocks hosted in the Puchang complex.

(3) Because the Puchang magma chamber has experienced a significantly longer differentiation history than the Wajilitag chamber, the former

residual magma gradually became more enriched in TFeO, and TiO_2. Unlike the Wajilitag complex, the wall rock of the Puchang complex is carbonates, which was likely to contain significant H_2O. It may be reasonable to suggest that there is external water intruded into the Puchang shallow chamber during plenty of Fe–Ti oxide crystallization (Fig. 15c). These processes would be sufficient to allow for the extensive Fe–Ti oxide crystallization and accumulation and subsequently resulted in effectively gravitational resorting and setting of the Fe–Ti oxide crystals, in clear contrast to the differentiation processes of the Wajilitag magma chamber (Fig. 15e).

(4) Due to the density contrast between Fe–Ti oxide crystals and silicate minerals, the high–density Fe–Ti oxide crystal slurries sorted during settling to form high–grade Fe–Ti oxide ores (e.g., massive oxide ores), and then settled downward as sills, lenses and pods, crosscutting the semi–solid cumulate rocks that occurs below them, and occurred at various stratigraphic levels in the gabbroic section with unconformable contacts (Fig. 15c). Meanwhile, these processes allow for more effective removal of the evolved interstitial liquid, and expel the evolved liquid out of the Puchang slowly cooling magma chamber. By contrast, Fe–Ti oxide crystals in the Wajilitag magma chamber may crystallize from Fe–Ti rich liquids that probably co–existed with silicate minerals and could be only concentrated as disseminated, either concordant or discordant, oxide ore bodies in early–formed cumulate clinopyroxenites or at the base of the gabbros with no distinct boundaries (Fig. 15f).

6. Conclusions

(1) The Puchang marginal zone rocks may represent samples of evolved fractionates of the parental magma and not of this magma itself. The Fe–Ti–rich parental magma for the Puchang complex is more evolved than that for the Wajilitag complex. The ferrobasalt parental magmas could be probably generated by partial melting of the enriched subcratonic lithosphere mantle that has incorporated subduction-related components in response to

the impingement of the inferred mantle plume.

(2) Lithologic and element geochemical variations indicate that the Wajilitag and Puchang complexes may have experienced significantly different sequences of crystallization after emplacement of high–Fe–Ti basaltic magmas. These differences suggest that the arrival of Fe–Ti oxides in Wajilitag magmatic system relatively earlier than that in Puchang magmatic system during the course of differentiation. The relatively earlier onset of Fe–Ti oxide crystallization in the Wajilitag magma could be interpreted to be the result of the high TFeO and TiO_2 contents of the parental magma.

(3) The Fe–Ti oxide ores in above complexes most probably result from normal fractional crystallization and cumulus processes of basaltic melts in relatively closed systems. The protracted differentiation history of Fe highly enriched parental magma and the introduction of external H_2O from the wall rock could be key factors for the crystallization and accumulation of abundant Fe–Ti oxides and the formation of massive ores in this case.

Supplementary data associated with this article can be found, in the online version, at doi: ….

Acknowledgments

Constructive reviews and suggestions by Dr. Geoffrey Howarth and one anonymous reviewer helped to improve the revised version. The editorial suggestions of Dr. Nelson Eby helped to improve the revised version. Prof. Chusi Li is thanked for comments on an earlier version of this manuscript. Thanks are given to Mr. Donglin Ma and Mr. Jun Cheng of the Wajilitag mine, Mr. Xu of the Puchang mine, Ms. Jianli Kang of the Tianjin Institute of Geology and Mineral Resources, who kindly allowed us to acquire samples for this study and gave all facilities for the mine trip. We are grateful to Dr. Yongsheng Li for useful discussion about reliability of the modeling software, Drs. Yinxi Wang, Suohan Tang, and He Li for assistance in geochemical analyzes, Dr.

Zhenyu Chen and Dr. Jingwu Yin for assistance in electron microprobe analyzes. This research was jointly supported by the National Basic Research Program of China (973 Program, No. 2012CB416806), National Natural Science Foundation of China (No. 41602055), and 305 Project of the State Science and technology Program of China (Nos. 2007BAB25B05 and 2011BAB06B02–04).

Figure captions

Fig. 1. (a) Early Permian (ca. 280 Ma) paleogeographic reconstructions showing the locations of Tarim LIP, Panjal Traps, Siberian Traps and Emeishan LIP in the world (modified from Li and Powell, 2001). **(b)** Simplified tectonic map of the Tarim Craton and surrounding areas showing the distribution of Permian basalts and the locations of the Fe–Ti oxide ore–bearing complexes in the Tarim Craton (modified from Tian et al., 2010).

Fig. 2. Simplified geological maps and cross sections of the Wajilitag complex, with locations of investigated drill core and sample (modified from XJGMR, 1984).

Fig. 3. Simplified geological maps and cross sections of the Puchang complex, with locations of investigated drill core and sample (modified from XJGMR, 2010).

Fig. 4. Field photographs and photomicrographs of the Wajilitag rocks and ores. **(a)** Cumulus clinopyroxene with Fe–Ti oxides in clinopyroxenite under plane–polarized light, transmitted light. **(b)** Cumulus olivine and clinopyroxene with Fe–Ti oxide in clinopyroxenite under plane–polarized light, transmitted light. **(c, d)** Clinopyroxene and plagioclase with Fe–Ti oxide in gabbro under crossed polars, transmitted light. **(e)** Olivine and clinopyroxene phenocrysts in

gabbro, and Fe–Ti oxide inclusions in a clinopyroxene grain under crossed polars, transmitted light. **(f)** Clinopyroxene and olivine in the disseminated ore under plane–polarized light, transmitted light. Note that olivine grains enclosed in large clinopyroxene crystal. Mineral abbreviations: Ol, olivine; Cpx, clinopyroxene; Pl, plagioclase.

Fig. 5. Backscattered electron (BSE) images of the Wajilitag rocks and ores. **(a, b)** Olivine, clinopyroxene, plagioclase and magnetite with ilmenite lamellae in the clinopyroxenite. Some sub–round magnetite enclosed in clinopyroxene and olivine crystals. **(c)** The Fe–Ti oxides occur as euhedral or rounded inclusions in silicate minerals or as anhedral grains between silicate minerals in the gabbro. Mineral abbreviations: Mt, magnetite; Ilm, ilmenite; other abbreviations as in Fig. 4.

Fig. 6. Field photographs and photomicrographs of the Puchang rocks and ores. **(a)** Intrusive contact of plagioclase–bearing clinopyroxenite with the Kangkelin Formation (marble). **(b)** Sharp boundary of disseminated ore and gabbro. **(c)** Thin tabular sheets of massive ore in sharp contact with disseminated ore. **(d)** Centimeter–scale bands of massive ore appear intact within disseminated ore. **(e)** Representative outcrop of a centimeter–scale disseminated Fe–Ti oxide layer. **(f)** Plagioclase–bearing clinopyroxenite consisting of cumulus clinopyroxene with interstitial plagioclase under crossed polars, transmitted light; the presence of clinopyroxene grain with straight to slightly curved boundaries with distinct triple junctions (arrow) should be noted. **(g)** Gabbro consisting of cumulus clinopyroxene and plagioclase surrounded by ‘interstitial’ Fe–Ti oxides under crossed polars, transmitted light; planar foliation and lineation defined by orientation of long lath–shaped plagioclase and tabular clinopyroxene. **(h)** Cumulus olivine, clinopyroxene and plagioclase with ‘interstitial’ Fe–Ti oxides in gabbro under plane–polarized light, transmitted light. **(i)** Cumulus plagioclase with olivine and clinopyroxene in the

anorthosite under crossed polars, transmitted light. Note clinopyroxene reaction rims between plagioclase and olivine. **(j)** Clinopyroxene and plagioclase with distinct hornblende rims surrounded by Fe–Ti oxides in the disseminated ore. The thin black lines within the silicate minerals are exsolution of oxides under plane–polarized light, transmitted light. **(k)** Isolated olivine and plagioclase grains in the massive ore under plane–polarized light, transmitted light. Hornblende is commonly present as monomineralic rims at the contact of Fe–Ti oxides and embayed olivine or plagioclase. **(l)** The magnetites often show exsolved ilmenite lamellae, minor sulfides are sparsely disseminated both in the silicate minerals and the Fe–Ti oxides in the massive ore under plane–polarized light, reflected light. Mineral abbreviations: Hb, Hornblende; Sul, sulfide; other abbreviations as in Fig. 4.

Fig. 7. BSE images of the Puchang rocks. Magnetite crystals occur as euhedral or sub–rounded grains enclosed in silicate minerals or as interstitial phases between silicate minerals. Note that many magnetite grains exhibit complex ilmenite subsolidus exsolution lamellae and ilmenite grains are free of exsolution and sparse sulfide grains occur as interstitial phases. Mineral abbreviations: Po, Pyrrhotite; other abbreviations as in Figs. 4 and 5.

Fig. 8. Variation diagrams of olivine and clinopyroxene from the Wajilitag and Puchang various ores/rocks. **(a)** NiO versus Fo of olivine (Ol); **(b)** Cr_2O_3 versus $Mg^{\#}$ of clinopyroxene (Cpx); **(c)** TiO_2 versus $Mg^{\#}$ of Cpx. Data are from this study and previous studies given in Supplementary Data Electronic Appendices 2–3.

Fig. 9. Histograms showing the distribution of An contents of plagioclase (Pl) from the Wajilitag and Puchang various ores/rocks. The full dataset is given in Supplementary Data Electronic Appendix 4.

Fig. 10. Variation diagrams of Fe–Ti oxides from the Wajilitag and Puchang various ores/rocks. MgO **(a)**, Cr_2O_3 **(b)** versus TiO_2 of magnetite (Mt); **(c)** MgO versus TiO_2 of ilmenite (Ilm). Data are from this study and previous studies given in Supplementary Data Electronic Appendices 5–6.

Fig. 11. Variation diagrams for representative major elements. SiO_2 **(a)**, Al_2O_3 **(b)**, TiO_2 **(c)**, TFeO **(d)**, CaO **(e)**, Na_2O+K_2O **(f)** and P_2O_5 **(g)** versus MgO, respectively; TFe_2O_3 versus TiO_2 **(h)** for different types of rocks from the Wajilitag and Puchang complexes. Data are from this study and previous studies given in Supplementary Data Electronic Appendix 7.

Fig. 12. Primitive mantle–normalized trace element patterns and chondrite–normalized rare earth element (REE) patterns of the Wajilitag and Puchang intrusive rocks and ores. Data are from this study and previous studies given in Supplementary Data Electronic Appendix 7. The solid and open symbols (i.e., circles and squares) represent data from the present study and previous studies, respectively. Normalization values and average ocean–island basalt (OIB) pattern are from Sun and McDonough (1989). Data for the mafic dyke samples (W13 and ZK4–2–15–3) are from Jiang et al. (2004b) and the authors' unpublished results, respectively.

Fig. 13. Diagram of I_{Sr} versus $\varepsilon_{Nd}(t)$ for the Wajilitag and Puchang intrusive rocks and ores. Data sources: DM, MORB and OIB (Zindler and Hart, 1986); Kimberlitic rocks and their hosted xenoliths (Zhang et al., 2013 and references therein); early Permian basalts (Li et al., 2012b; Tian et al., 2010; Zhang et al., 2010 and references therein); Late Neoarchean and early Paleoproterozoic basement (Long et al., 2011; Zhang et al., 2008, 2012a). I_{Sr} and $\varepsilon_{Nd}(t)$ for these previously published data recalculated to 280 Ma. Numbers labeled on the mixing curves are the percentages of participation of the crustal materials. The calculated parameters of Sr (ppm), Nd (ppm), I_{Sr} and $\varepsilon_{Nd}(t)$ are 255, 8.18,

0.7038 and +5.25 from the kimberlitic intrusion–hosted xenolith sample (W10–97) as presumed parental magma (Jiang et al., 2004a). Tarim carbonates (255 ppm Sr, 1.0 ppm Nd, I_{Sr}=0.7038 and $\varepsilon_{Nd}(t)$=–26; Li et al., 2011), Mid–Paleozoic granties (614 ppm Sr, 61.5 ppm Nd, I_{Sr}=0.7092 and $\varepsilon_{Nd}(t)$=–8.46; Huang et al., 2013), Neoproterozoic granties (595 ppm Sr, 36.6 ppm Nd, I_{Sr}=0.7115 and $\varepsilon_{Nd}(t)$=–21.25; Cao et al., 2011) and grabbros (661 ppm Sr, 21.6 ppm Nd, I_{Sr}=0.7129 and $\varepsilon_{Nd}(t)$=–9.18; Zhang et al., 2012b) as four components of the Tarim middle/upper crust. Symbols as in Fig. 8.

Fig. 14. Modeling results of the proposed liquid lines of descent for the Wajilitag **(a)** and Puchang **(b)** parental magmas. Calculation has been performed by PELE software (Boudreau, 1999) using model assumptions reported in the text.

Fig. 15. Schematic cartoon illustrating the postulated formation processes of the various rock types and associated Fe–Ti oxide ores in the Wajilitag and Puchang complexes. Detail comments as described within the text.

Table captions

Table 1: Samples and brief description

Table 2: Representative Sr–Nd isotopic compositions for whole rocks and clinopyroxene separates from the Wajilitag and Puchang intrusive rocks

Table 3: Major (wt.%) element compositions of the Wajilitag and Puchang inferred parental magmas and comparison with parental magma compositions of other oxide ore–bearing mafic–ultramafic intrusions

Table 4: Composition of silicate minerals at the onset of Fe–Ti oxide crystallization in the Wajilitag and Puchang complexes compared to several

typical mafic–untralmafic intrusions

References

Bai, Z.J., Zhong, H., Li, C.S., Zhu, W.G., He, D.F., Qi, L., 2014. Contrasting parental magma compositions for the Hongge and Panzhihua magmatic Fe-Ti-V oxide deposits, Emeishan Large Igneous Province, SW China. Economic Geology 109, 1763-1785.

Bai, Z.J., Zhong, H., Naldrett, A.J., Zhu, W.G., Xu, G.W., 2012. Whole-rock and mineral composition constraints on the genesis of the giant Hongge Fe-Ti-V oxide deposit in the Emeishan Large Igneous Province, Southwest China. Economic Geology 107, 507-524.

Berndt, J., Koepke, J., Holtz, F., 2005. An experimental investigation of the influence of water and oxygen fugacity on differentiation of MORB at 200 MPa. Journal of Petrology 46, 135-167.

Botcharnikov, R.E., Almeev, R.R., Koepke, J., Holtz, F., 2008. Phase relations and liquid lines of descent in hydrous ferrobasalt—implications for the Skaergaard intrusion and Columbia river flood basalts. Journal of Petrology 49, 1687-1727.

Boudreau, A.E., 1999. PELE—a version of the MELTS software program for the PC platform. Computers & Geosciences 25, 201-203.

Cao, J., Wang, C.Y., Xing, C.M., Xu, Y.G., 2014. Origin of the early Permian Wajilitag igneous complex and associated Fe-Ti oxide mineralization in the Tarim large igneous province, NW China. Journal of Asian Earth Sciences 84, 51–68.

Cao, X.F., Lü, X.B., Liu, S.T., Zhang, P., Gao, X., Chen, C., Mo, Y.L., 2011. LA-ICP-MS zircon dating, geochemistry, petrogenesis and tectonic implications of the Dapingliang Neoproterozoic granites at Kuluketage block, NW China. Precambrian Research 186, 205-219.

Charlier, B., Duchesne, J.C., Vander Auwera, J., 2006. Magma chamber processes in the Tellnes ilmenite deposit (Rogaland Anorthosite Province, SW Norway) and the formation of Fe–Ti ores in massif-type anorthosites. Chemical Geology 234, 264-290.

Charlier, B., Grove, T.L., 2012. Experiments on liquid immiscibility along tholeiitic liquid lines of descent. Contributions to Mineralogy and Petrology 164, 27-44.

Charlier, B., Namur, O., Toplis, M.J., Schiano, P., Cluzel, N., Higgins, M.D., Vander Auwera, J., 2011. Large-scale silicate liquid immiscibility during differentiation of tholeiitic basalt to granite and the origin of the Daly gap. Geology 39, 907-910.

Chen, F., Siebel, W., Satir, M., Terzioğlu, M., Saka, K., 2002. Geochronology of the Karadere basement (NW Turkey) and implications for the geological evolution of the Istanbul zone. International Journal of Earth Sciences 91, 469-481.

DePaolo, D.J., 1981. Trace element and isotopic effects of combined wallrock assimilation and fractional crystallization. Earth and Planetary Science Letters 53, 189-202.

Eales, H.V., Costin, G., 2012. Crustally contaminated komatiite: primary source of the chromitites and Marginal, Lower, and Critical Zone magmas in a staging chamber beneath the Bushveld Complex. Economic Geology 107, 645-665.

Ernst, R.E., Jowitt, S.M., 2013. Large igneous provinces (LIPs) and metallogeny. Society of Economic Geologists Special Publication 17, 17–51.

Falloon, T.J., Danyushevsky, L.V., 2000. Melting of refractory mantle at 1· 5, 2 and 2· 5 GPa under anhydrous and H2O-undersaturated conditions: implications for the petrogenesis of high-Ca boninites and the influence of subduction components on mantle melting. Journal of Petrology 41, 257-283.

Fischer, L.A., Wang, M., Charlier, B., Namur, O., Roberts, R.J., Veksler, I.V., Cawthorn, R.G., Holtz, F., 2016. Immiscible iron- and silica-rich liquids in the Upper Zone of the Bushveld Complex. Earth and Planetary Science Letters 443, 108-117.

Frey, F.A., Green, D.H., Roy, S.D., 1978. Integrated models of basalt petrogenesis: a study of quartz tholeiites to olivine melilitites from south eastern Australia utilizing geochemical and experimental petrological data. Journal of petrology 19, 463-513.

Ganino, C., Arndt, N.T., Zhou, M.F., Gaillard, F., Chauvel, C., 2008. Interaction of magma with sedimentary wall rock and magnetite ore genesis in the Panzhihua mafic intrusion, SW China. Mineralium Deposita 43, 677-694.

Howarth, G.H., Harris, C., 2017. Discriminating between pyroxenite and peridotite sources for continental flood basalts (CFB) in southern Africa using olivine chemistry. Earth and Planetary Science Letters 475, 143-151.

Howarth, G.H., Prevec, S.A., 2013a. Hydration vs. oxidation: Modelling implications for Fe-Ti

oxide crystallisation in mafic intrusions, with specific reference to the Panzhihua intrusion, SW China. Geoscience Frontiers 4, 555-569.

Howarth, G.H., Prevec, S.A., 2013b. Trace Element, PGE, and Sr-Nd isotope geochemistry of the Panzhihua mafic layered intrusion, SW China: Constraints on ore-forming processes and evolution of parent magma at depth in a plumbing-system. Geochimica et Cosmochimica Acta 120, 459-478.

Howarth, G.H., Prevec, S.A., Zhou, M.F., 2013. Timing of Ti-magnetite crystallisation and silicate disequilibrium in the Panzhihua mafic layered intrusion: Implications for ore-forming processes. Lithos 170-171, 73–89.

Huang, H., Zhang, Z.C., Kusky, T., Santosh, M., Zhang, S., Zhang, D.Y., Liu, J.L., Zhao, Z.D., 2012. Continental vertical growth in the transitional zone between South Tianshan and Tarim, western Xinjiang, NW China: Insight from the Permian Halajun A1-type granitic magmatism. Lithos 155, 49-66.

Huang, H., Zhang, Z.C., Santosh, M., Zhang, D.Y., Zhao, Z.D., Liu, J.L., 2013. Early Paleozoic tectonic evolution of the South Tianshan Collisional Belt: Evidence from geochemistry and zircon U-Pb geochronology of the Tie'reke monzonite pluton, northwest China. The Journal of Geology 121, 401-424.

Jiang, C.Y., Zhang, P.B., Lu, D.R., Bai, K.Y., 2004a. Petrogenesis and magma source of the ultramafic rocks at Wajilitag region, western Tarim Plate in Xinjiang. Acta Petrologica Sinica 20, 1433-1444 (in Chinese with English abstract).

Jiang, C.Y., Zhang, P.B., Lu, D.R., Bai, K.Y., 2004b. Source of the Fe- enriched-type high-Mg magma in Mazhartag region, Xinjiang. Acta Geologica Sinica 78, 770–780 (in Chinese with English abstract).

Jugo, P.J., 2005. An experimental study of the sulfur content in basaltic melts saturated with immiscible sulfide or sulfate liquids at 1300 C and 1.0 GPa. Journal of Petrology 46, 783-798.

Juster, T.C., Grove, T.L., Perfit, M.R., 1989. Experimental constraints on the generation of FeTi basalts, andesites, and rhyodacites at the Galapagos Spreading Center, 85°W and 95°W. Journal of Geophysical Research 94, 9251-9274.

Li, P.C., Chen, G.H., Zeng, Q.S., Yi, J., Hu, G., 2011. Genesis of Lower Ordovician dolomite in

Central Tarim Basin. Acta Sedimentologica Sinica 29, 842-856 (in Chinese with English abstract).

Li, Y.Q., Li, Z.L., Chen, H.L., Yang, S.F., Yu, X., 2012a. Mineral characteristics and metallogenesis of the Wajilitag layered mafic–ultramafic intrusion and associated Fe–Ti–V oxide deposit in the Tarim large igneous province, northwest China. Journal of Asian Earth Sciences 49, 161-174.

Li, Z.L., Li, Y.Q., Chen, H.L., Santosh, M., Yang, S.F., Xu, Y.G., Langmuir, C.H., Chen, Z.X., Yu, X., Zou, S.Y., 2012b. Hf isotopic characteristics of the Tarim Permian large igneous province rocks of NW China: Implication for the magmatic source and evolution. Journal of Asian Earth Sciences 49, 191-202.

Li, Z.X., Powell, C.M.A., 2001. An outline of the palaeogeographic evolution of the Australasian region since the beginning of the Neoproterozoic. Earth-Science Reviews 53, 237-277.

Liu, P.P., Zhou, M.F., Chen, W.T., Boone, M., Cnudde, V., 2014. Using multiphase solid inclusions to constrain the origin of the Baima Fe–Ti–(V) oxide deposit, SW China. Journal of Petrology 55, 951-976.

Long, X.P., Yuan, C., Sun, M., Kröner, A., Zhao, G.C., Wilde, S., Hu, A.Q., 2011. Reworking of the Tarim Craton by underplating of mantle plume-derived magmas: Evidence from Neoproterozoic granitoids in the Kuluketage area, NW China. Precambrian Research 187, 1-14.

Mathison, C.I., Ahmat, A.L., 1996. The Windimurra Complex, Western Australia, in: Cawthorn, R.G. (Ed.), Layered Intrusions. Developments in Petrology. Elsevier, Amsterdam, pp. 485-510.

Namur, O., Charlier, B., Toplis, M.J., Higgins, M.D., Liégeois, J.P., Vander Auwera, J., 2010. Crystallization sequence and magma chamber processes in the ferrobasaltic Sept Iles layered intrusion, Canada. Journal of Petrology 51, 1203-1236.

Pang, K.N., Li, C.S., Zhou, M.F., Ripley, E.M., 2008a. Abundant Fe–Ti oxide inclusions in olivine from the Panzhihua and Hongge layered intrusions, SW China: evidence for early saturation of Fe–Ti oxides in ferrobasaltic magma. Contributions to Mineralogy and Petrology 156, 307-321.

Pang, K.N., Li, C.S., Zhou, M.F., Ripley, E.M., 2009. Mineral compositional constraints on

petrogenesis and oxide ore genesis of the late Permian Panzhihua layered gabbroic intrusion, SW China. Lithos 110, 199-214.

Pang, K.N., Shellnutt, J.G., Zhou, M.F., 2015. The Panzhihua intrusion, SW China, in: Charlier, B., Namur, O., Latypov, R., Tegner, C. (Eds.), Layered Intrusions. Springer Netherlands, pp. 435-463.

Pang, K.N., Zhou, M.F., Lindsley, D., Zhao, D.G., Malpas, J., 2008b. Origin of Fe-Ti oxide ores in mafic intrusions: Evidence from the Panzhihua intrusion, SW China. Journal of Petrology 49, 295-313.

Prokoph, A., El Bilali, H., Ernst, R., 2013. Periodicities in the emplacement of large igneous provinces through the Phanerozoic: Relations to ocean chemistry and marine biodiversity evolution. Geoscience Frontiers 4, 263-276.

Qi, L., Hu, J., Gregoire, D.C., 2000. Determination of trace elements in granites by inductively coupled plasma mass spectrometry. Talanta 51, 507-513.

Qu, J.F., Xiao, W.J., Windley, B.F., Han, C.M., Mao, Q.G., Ao, S.J., Zhang, J.E., 2011. Ordovician eclogites from the Chinese Beishan: implications for the tectonic evolution of the southern Altaids. Journal of Metamorphic Geology 29, 803-820.

Roeder, P.L., Emslie, R.F., 1970. Olivine-liquid equilibrium. Contributions to mineralogy and petrology 29, 275-289.

Shellnutt, J.G., 2014. The Emeishan large igneous province: A synthesis. Geoscience Frontiers 5, 369–394.

Shellnutt, J.G., Bhat, G.M., Brookfield, M.E., Jahn, B.M., 2011. No link between the Panjal Traps (Kashmir) and the Late Permian mass extinctions. Geophysical Research Letters 38, doi:10.1029/2011GL049032.

Shellnutt, J.G., Pang, K.N., 2012. Petrogenetic implications of mineral chemical data for the Permian Baima igneous complex, SW China. Mineralogy and Petrology 106, 75-88.

Snyder, D., Carmichael, I.E., Wiebe, R.A., 1993. Experimental study of liquid evolution in an Fe-rich, layered mafic intrusion: constraints of Fe-Ti oxide precipitation on the T-fO 2 and T-ϱ paths of tholeiitic magmas. Contributions to Mineralogy and Petrology 113, 73-86.

Song, X.Y., Qi, H.W., Hu, R.Z., Chen, L.M., Yu, S.Y., Zhang, J.F., 2013. Formation of thick stratiform Fe-Ti oxide layers in layered intrusion and frequent replenishment of

fractionated mafic magma: Evidence from the Panzhihua intrusion, SW China. Geochemistry, Geophysics, Geosystems 14, 712-732.

Sun, S.S., McDonough, W., 1989. Chemical and isotopic systematics of oceanic basalts: implications for mantle composition and processes. Geological Society, London, Special Publications 42, 313-345.

Tang, Q.Y., Li, C.S., Tao, Y., Ripley, E.M., Xiong, F., 2017. Association of Mg-rich olivine with magnetite as a result of brucite marble assimilation by basaltic magma in the Emeishan Large Igneous Province, SW China. Journal of Petrology 58, 699-714.

Tegner, C., Cawthorn, R.G., Kruger, F.J., 2006. Cyclicity in the main and upper zones of the Bushveld complex, South Africa: Crystallization from a zoned magma sheet. Journal of Petrology 47, 2257-2279.

Thompson, R.N., Gibson, S.A., 1994. Magmatic expression of lithospheric thinning across continental rifts. Tectonophysics 233, 41-68.

Tian, W., Campbell, I.H., Allen, C.M., Guan, P., Pan, W.Q., Chen, M.M., Yu, H.J., Zhu, W.P., 2010. The Tarim picrite–basalt–rhyolite suite, a Permian flood basalt from northwest China with contrasting rhyolites produced by fractional crystallization and anatexis. Contributions to Mineralogy and Petrology 160, 407-425.

Toplis, M.J., Carroll, M.R., 1995. An experimental study of the influence of oxygen fugacity on Fe-Ti oxide stability, phase relations, and mineral—melt equilibria in ferro-basaltic systems. Journal of Petrology 36, 1137-1170.

Tuff, J., Takahashi, E., Gibson, S., 2005. Experimental constraints on the role of garnet pyroxenite in the genesis of high-Fe mantle plume derived melts. Journal of Petrology 46, 2023-2058.

VanTongeren, J.A., Mathez, E.A., 2012. Large-scale liquid immiscibility at the top of the Bushveld Complex, South Africa. Geology 40, 491-494.

Veksler, I.V., Dorfman, A.M., Borisov, A.A., Wirth, R., Dingwell, D.B., 2007. Liquid immiscibility and the evolution of basaltic magma. Journal of Petrology 48, 2187-2210.

Wilson, J.R., Robins, B., Nielsen, F.M., Duchesne, J.C., Vander Auwera, J., 1996. The Bjerkreim-Sokndal layered intrusion, Southwest Norway, in: Cawthorn, R.G. (Ed.), Layered Intrusions. Developments in Petrology. Elsevier, Amsterdam, pp. 231-255.

Wilson, M., 1989. Igneous petrogenesis: a global tectonic approach, Unwin Hyman, London, p. 466.

XJGMR (Xinjiang Bureau of Geology and Mineral Resources), 1984. Geological map of Wajilitag area in Bachu county, Xinjiang, Scale 1:5000. Unpublished data (in Chinese).

XJGMR (Xinjiang Bureau of Geology and Mineral Resources), 2010. Geological map of Liuyongtag area in Atushi city, Xinjiang, Scale 1:10000. Unpublished data (in Chinese).

Xu, Y.G., Wei, X., Luo, Z.Y., Liu, H.Q., Cao, J., 2014. The Early Permian Tarim Large Igneous Province: Main characteristics and a plume incubation model. Lithos 204, 20–35.

Yaxley, G.M., 2000. Experimental study of the phase and melting relations of homogeneous basalt+peridotite mixtures and implications for the petrogenesis of flood basalts. Contributions to Mineralogy and Petrology 139, 326-338.

Yaxley, G.M., Sobolev, A.V., 2007. High-pressure partial melting of gabbro and its role in the Hawaiian magma source. Contributions to Mineralogy and Petrology 154, 371-383.

Zhang, C.L., Li, H.K., Santosh, M., Li, Z.X., Zou, H.B., Wang, H.Y., Ye, H.M., 2012a. Precambrian evolution and cratonization of the Tarim Block, NW China: Petrology, geochemistry, Nd-isotopes and U–Pb zircon geochronology from Archaean gabbro-TTG–potassic granite suite and Paleoproterozoic metamorphic belt. Journal of Asian Earth Sciences 47, 5-20.

Zhang, C.L., Li, X.H., Li, Z.X., Ye, H.M., Li, C.N., 2008. A Permian layered intrusive complex in the western Tarim block, northwestern China: product of a ca. 275–Ma mantle plume? The Journal of Geology 116, 269-287.

Zhang, C.L., Xu, Y.G., Li, Z.X., Wang, H.Y., Ye, H.M., 2010. Diverse Permian magmatism in the Tarim Block, NW China: Genetically linked to the Permian Tarim mantle plume? Lithos 119, 537-552.

Zhang, C.L., Zou, H.B., Wang, H.Y., Li, H.K., Ye, H.M., 2012b. Multiple phases of the Neoproterozoic igneous activity in Quruqtagh of the northeastern Tarim Block, NW China: Interaction between plate subduction and mantle plume? Precambrian Research 222-223, 488-502.

Zhang, D.Y., Zhang, Z.C., Encarnación, J., Xue, C.J., Duan, S.G., Zhao, Z.D., Liu, J.L., 2012c. Petrogenesis of the Kekesai composite intrusion, western Tianshan, NW China:

Implications for tectonic evolution during late Paleozoic time. Lithos 146-147, 65-79.

Zhang, D.Y., Zhang, Z.C., He, H., Encarnación, J., Zhou, N.W., Ding, X.X., 2014. Platinum-group elemental and Re–Os isotopic geochemistry of the Wajilitag and Puchang Fe–Ti–V oxide deposits, northwestern Tarim Large Igneous Province. Ore Geology Reviews 57, 589-601.

Zhang, D.Y., Zhang, Z.C., Mao, J.W., Huang, H., Cheng, Z.G., 2016. Zircon U–Pb ages and Hf–O isotopic signatures of the Wajilitag and Puchang Fe–Ti oxide–bearing intrusive complexes: Constraints on their source characteristics and temporal–spatial evolution of the Tarim large igneous province. Gondwana Research 37, 71-85.

Zhang, D.Y., Zhang, Z.C., Santosh, M., Cheng, Z.G., He, H., Kang, J.L., 2013. Perovskite and baddeleyite from kimberlitic intrusions in the Tarim large igneous province signal the onset of an end-Carboniferous mantle plume. Earth and Planetary Science Letters 361, 238-248.

Zhang, Z.C., Mahoney, J.J., Mao, J.W., Wang, F.S., 2006. Geochemistry of picritic and associated basalt flows of the western Emeishan flood basalt province, China. Journal of Petrology 47, 1997-2019.

Zhang, Z.C., Mao, J.W., Saunders, A.D., Ai, Y., Li, Y., Zhao, L., 2009. Petrogenetic modeling of three mafic–ultramafic layered intrusions in the Emeishan large igneous province, SW China, based on isotopic and bulk chemical constraints. Lithos 113, 369-392.

Zhao, Z.Y., Zhang, Z.C., Santosh, M., Huang, H., Cheng, Z.G., Ye, J.C., 2015. Early Paleozoic magmatic record from the northern margin of the Tarim Craton: Further insights on the evolution of the Central Asian Orogenic Belt. Gondwana Research 28, 328–347.

Zindler, A., Hart, S.R., 1986. Chemical geodynamics. Annual review of earth and planetary sciences 14, 493-571.

Table 1

Sample no.	Locality	Depth in core (m)	Latitude (N)	Longitude (E)	Lithology	Estimated modal mineralogy (vol.%)			
						Olivine	Clinopyroxene	Plagioclase	Fe–Ti oxides
ZK4503-1	Wajilitag	1	39°32'01"	78°56'06"	Melagabbro	0	60	24	15
ZK4503-7	Wajilitag	37	39°32'01"	78°56'06"	Clinopyroxenite	2	80	0	17
ZK4503-9	Wajilitag	46	39°32'01"	78°56'06"	Clinopyroxenite	20	59	3	16
ZK4503-15	Wajilitag	70	39°32'01"	78°56'06"	Clinopyroxenite	0	74	5	20
ZK4503-20	Wajilitag	105	39°32'01"	78°56'06"	Disseminated oxide ore/Oxide melagabbro	0	44	18	37
ZK4503-21	Wajilitag	113	39°32'01"	78°56'06"	Melagabbro	5	59	20	14
ZK4503-23	Wajilitag	125	39°32'01"	78°56'06"	Clinopyroxenite	5	75	3	15
ZK4503-24	Wajilitag	130	39°32'01"	78°56'06"	Clinopyroxenite	0	73	5	20
ZK4503-31	Wajilitag	170	39°32'01"	78°56'06"	Disseminated oxide ore/Oxide Clinopyroxenite	0	64	0	35
ZK4503-34	Wajilitag	185	39°32'01"	78°56'06"	Disseminated oxide ore/Oxide Clinopyroxenite	0	63	0	36
ZK4503-39	Wajilitag	218	39°32'01"	78°56'06"	Clinopyroxenite	0	79	0	20
ZK4503-43	Wajilitag	235	39°32'01"	78°56'06"	Disseminated oxide ore/Oxide Clinopyroxenite	3	66	0	30
ZK4503-45	Wajilitag	250	39°32'01"	78°56'06"	Disseminated oxide ore/Oxide Clinopyroxenite	1	56	0	42
ZK4503-47	Wajilitag	265	39°32'01"	78°56'06"	Disseminated oxide ore/Oxide Clinopyroxenite	0	28	0	71
ZK4503-50	Wajilitag	277	39°32'01"	78°56'06"	Disseminated oxide ore/Oxide Clinopyroxenite	5	54	5	35
ZK4503-52	Wajilitag	290	39°32'01"	78°56'06"	Clinopyroxenite	0	79	0	19
K-0	Wajilitag	–	39°32'08"	78°55'51"	Melagabbro	0	47	38	13
D44	Wajilitag	–	39°32'59"	78°55'55"	Melagabbro	0	37	57	4
D44-2	Wajilitag	–	39°32'59"	78°55'55"	Melagabbro	0	38	56	5
D52-1	Wajilitag	–	39°33'50"	78°56'11"	Clinopyroxenite	0	88	4	6
D52-25	Wajilitag	–	39°33'51"	78°56'09"	Melagabbro	0	51	40	7
D53	Wajilitag	–	39°32'02"	78°56'02"	Disseminated oxide ore/Oxide Clinopyroxenite	0	63	0	36
DW24-3	Wajilitag	–	39°31'58"	78°56'04"	Disseminated oxide ore/Oxide Clinopyroxenite	1	62	1	35
DW24-4	Wajilitag	–	39°31'58"	78°56'04"	Clinopyroxenite	1	77	1	19
DW26-1	Wajilitag	–	39°32'06"	78°56'07"	Disseminated oxide ore/Oxide Clinopyroxenite	1	57	0	41
DW27-1	Wajilitag	–	39°32'06"	78°56'07"	Disseminated oxide ore/Oxide melagabbro	0	45	20	34
DW27-2	Wajilitag	–	39°32'06"	78°56'07"	Disseminated oxide ore/Oxide Clinopyroxenite	0	53	2	44
DW27-5	Wajilitag	–	39°32'06"	78°56'07"	Melagabbro	0	49	34	15
DW28-2	Wajilitag	–	39°32'07"	78°56'07"	Disseminated oxide ore/Oxide melagabbro	0	33	31	35
DW33-1	Wajilitag	–	39°32'50"	78°55'38"	Melagabbro	3	25	60	10
ZK4-2-1	Puchang	3	40°26'33"	77°37'55"	Disseminated oxide ore	2	25	39	31
ZK4-2-4	Puchang	24	40°26'33"	77°37'55"	Gabbro	1	20	75	3

Table 1: Continued

Sample no.	Locality	Depth in core (m)	Latitude (N)	Longitude (E)	Lithology	Estimated modal mineralogy (vol.%)			
						Olivine	Clinopyroxene	Plagioclase	Fe–Ti oxides
ZK4-2-9-1	Puchang	61	40°26'33"	77°37'55"	Gabbro	25	16	52	5
ZK4-2-16-4	Puchang	108	40°26'33"	77°37'55"	Gabbro	1	39	49	9
ZK4-2-17-1	Puchang	114	40°26'33"	77°37'55"	Disseminated oxide ore	3	28	30	35
ZK4-2-17-2	Puchang	115	40°26'33"	77°37'55"	Disseminated oxide ore	2	32	35	25
ZK4-2-17-8	Puchang	119	40°26'33"	77°37'55"	Disseminated oxide ore	1	31	28	37
ZK4-2-19-3	Puchang	131	40°26'33"	77°37'55"	Gabbro	25	35	32	7
ZK4-2-21-1	Puchang	142	40°26'33"	77°37'55"	Disseminated oxide ore	5	43	15	35
ZK4-2-22-2	Puchang	150	40°26'33"	77°37'55"	Gabbro	25	32	39	3
D8-1	Puchang	–	40°25'48"	77°37'48"	Plagioclase–bearing clinopyroxenite	0	90	6	1
D8-3	Puchang	–	40°25'49"	77°37'49"	Plagioclase–bearing clinopyroxenite	0	92	5	1
D55-11	Puchang	–	40°26'32"	77°38'01"	Massive oxide ore	1	4	0	90
D55-12	Puchang	–	40°26'32"	77°38'01"	Gabbro	0	23	52	23
D55-18	Puchang	–	40°26'32"	77°38'01"	Disseminated oxide ore	2	5	49	42
D55-19	Puchang	–	40°26'32"	77°38'01"	Massive oxide ore	4	4	8	82
D56	Puchang	–	40°26'32"	77°38'03"	Disseminated ore	0	31	39	27
D56-1	Puchang	–	40°26'28"	77°38'22"	Anorthosite	2	3	90	3
D56-12	Puchang	–	40°26'32"	77°38'03"	Disseminated oxide ore	1	14	47	35
D56-18	Puchang	–	40°26'32"	77°38'03"	Disseminated oxide ore	1	14	48	36
D56-27	Puchang	–	40°26'34"	77°38'02"	Gabbro	2	30	55	11
D58	Puchang	–	40°26'36"	77°38'02"	Gabbro	0	24	70	5
D59-5	Puchang	–	40°27'05"	77°38'20"	Gabbro	2	17	73	6
D59-6	Puchang	–	40°27'05"	77°38'20"	Gabbro	2	17	73	6
D61-2	Puchang	–	40°26'44"	77°39'10"	Plagioclase–bearing clinopyroxenite	0	89	6	1
DP2-1	Puchang	–	40°26'32"	77°38'00"	Massive oxide ore	1	5	8	81
DP6-1	Puchang	–	40°26'45"	77°38'19"	Gabbro	1	10	84	3
DP6-2	Puchang	–	40°26'44"	77°38'21"	Anorthosite	2	5	90	2
DP11-1	Puchang	–	40°26'56"	77°38'19"	Anorthosite	0	5	92	2
NPC-11	Puchang	–	40°26'24"	77°36'28"	Gabbro	25	27	38	9
NPC-12	Puchang	–	40°26'12"	77°36'31"	Gabbro	1	23	64	10
NPC-14	Puchang	–	40°26'06"	77°36'30"	Anorthosite	5	3	87	4
NPC-15	Puchang	–	40°26'04"	77°36'31"	Anorthosite	0	4	93	1
NPC-16	Puchang	–	40°26'03"	77°36'31"	Anorthosite	0	9	88	2

Modal proportions (vol.%) have been determined by point counting. —, no information.

Table 2

Sample no.	Rock/ore-type	Sample type	Rb(ug/g)	Sr(ug/g)	$^{87}Rb/^{86}Sr$	$^{87}Sr/^{86}Sr$	2σ	$(^{87}Sr/^{86}Sr)_i$	Sm(ug/g)	Nd(ug/g)	$^{147}Sm/^{144}Nd$	$^{143}Nd/^{144}Nd$	2σ	$\varepsilon_{Nd}(t)$
Wajilitag complex														
ZK4503-7	Clinopyroxenite	Whole rock	0.9784	73.17	0.0387	0.70439	16	0.7042	4.221	14.58	0.1751	0.512685	11	1.70
ZK4503-9		Whole rock	2.224	110.5	0.0582	0.70495	20	0.7047	4.604	16.59	0.1679	0.512672	5	1.71
ZK4503-15		Whole rock	0.6052	53.91	0.0325	0.70485	24	0.7047	3.520	11.69	0.1821	0.512613	9	0.04
ZK4503-24		Whole rock	1.423	343.2	0.0120	0.70483	23	0.7048	6.653	25.85	0.1557	0.512641	10	1.54
D52-1		Whole rock	7.917	332.5	0.0689	0.70504	13	0.7048	11.67	57.32	0.1232	0.512535	7	0.65
DW24-4		Whole rock	1.879	72.00	0.0755	0.70459	18	0.7043	4.162	13.94	0.1806	0.512755	10	2.87
ZK4503-1	Melagabbro	Whole rock	1.838	434.0	0.0123	0.70481	15	0.7048	4.201	15.03	0.169	0.512668	9	1.59
D44-2		Whole rock	44.39	990.3	0.1296	0.70433	10	0.7038	12.43	63.34	0.1187	0.512643	6	2.92
DW27-5		Whole rock	1.176	605.6	0.0056	0.70427	21	0.7042	13.72	65.33	0.127	0.512663	9	3.01
K-0*		Whole rock	39.87	861.2	0.1446	0.70483	8	0.7042	12.75	71.23	0.1173	0.512521	8	0.59
ZK4503-45	Disseminated	Whole rock	0.7427	66.15	0.0325	0.70470	14	0.7046	3.671	12.80	0.1736	0.512626	10	0.60
DW26-1	ore	Whole rock	1.331	54.55	0.0706	0.70489	15	0.7046	4.047	13.53	0.181	0.512714	5	2.05
D53		Clinopyroxene	0.1492	79.51	0.0054	0.70420	12	0.7042	6.510	21.59	0.1824	0.512729	10	2.29
Puchang complex														
D8-3*	Clinopyroxenite	Whole rock	2.863	238.9	0.0357	0.70504	9	0.7049	9.987	52.36	0.1281	0.512635	9	2.35
D61-2		Whole rock	0.4194	65.82	0.0184	0.70786	15	0.7078	0.1554	0.3913	0.2402	0.512631	5	-1.67
ZK4-2-4	Gabbro	Whole rock	3.995	74.18	0.1558	0.70522	15	0.7046	1.116	4.239	0.1593	0.512591	9	0.40
DP6-1*		Whole rock	2.341	230.4	0.0269	0.70399	7	0.7039	1.234	3.897	0.1905	0.512726	7	1.94
NPC-11*		Whole rock	2.098	287.1	0.0208	0.70418	7	0.7041	1.956	5.809	0.1961	0.512681	6	0.86
NPC-12*		Whole rock	5.607	520.5	0.0315	0.70424	8	0.7041	2.113	8.453	0.1463	0.512586	9	0.76
D59-6		Clinopyroxene	0.5786	70.23	0.0238	0.70556	22	0.7055	3.366	9.702	0.2099	0.512668	11	0.12
D58		Clinopyroxene	1.368	65.98	0.0600	0.70608	16	0.7058	5.055	16.31	0.1875	0.512625	10	0.07
D56-1	Anorthosite	Whole rock	4.279	473.4	0.0261	0.70522	13	0.7051	1.026	4.847	0.1281	0.512529	10	0.28
NPC-14*		Whole rock	5.012	596.2	0.0226	0.70413	6	0.7040	1.306	4.516	0.1518	0.512598	7	0.80
NPC-15*		Whole rock	4.013	731.8	0.0164	0.70394	8	0.7039	1.014	5.198	0.1136	0.512601	8	2.20
ZK4-2-17-2	Disseminated	Whole rock	5.755	69.16	0.2407	0.70543	16	0.7045	2.659	9.450	0.1702	0.512582	9	-0.16
ZK4-2-21-1	ore	Whole rock	4.010	72.37	0.1603	0.70555	15	0.7049	2.093	11.09	0.1142	0.512484	8	-0.11
D55-12		Whole rock	1.297	312.4	0.0120	0.70563	14	0.7056	1.144	4.220	0.1641	0.512576	8	-0.06
D56-18		Clinopyroxene	1.396	73.77	0.0548	0.70566	20	0.7054	3.645	11.31	0.1949	0.512635	12	0.00
D56		Clinopyroxene	1.109	72.68	0.0441	0.70561	19	0.7054	3.740	11.57	0.1956	0.512637	6	0.02
D55-11	Massive ore	Whole rock	0.1489	16.20	0.0266	0.70593	21	0.7058	0.1783	0.5738	0.1879	0.51262	7	-0.04

*=samples analyzed at the Center of Materials analysis, Nanjing University; the remaining samples were analyzed at Institute of Geology, Chinese Academy of Geological Sciences. Supplementary Data Electronic Appendix 8 contains the full dataset.

Table 3

Sample no.	W13[1]	ZK4-2-15-3[2]					
Name	Wajilitag	Puchang	Hongge[3]	Panzhihua[4]	Taihe[5]	Skaergaard[6]	Sept Iles[7]
Rock type	Diabase	Gabbroic dyke					
SiO_2	46.74	49.20	47.28	44.70	50.45	48.82	48.56
TiO_2	2.91	2.74	3.51	2.78	2.61	2.24	2.85
Al_2O_3	10.11	14.29	9.93	15.27	12.36	14.42	14.50
TFe_2O_3	15.16	15.52	16.11	13.58	12.19	13.48	16.53
MnO	0.15	0.19	0.18	0.19	0.2	0.18	0.24
MgO	8.85	4.62	9.39	7.16	7.44	6.06	5.47
CaO	9.46	8.23	11.22	10.22	9.95	12.57	9.71
Na_2O	2.29	3.06	1.76	2.57	2.61	3.01	2.78
K_2O	0.16	1.18	1.15	1.41	1.41	0.38	0.78
P_2O_5	0.47	0.37	0.29	0.38	0.3	0.20	0.57
LOI	3.44	0.26	—	1.70	0.5	—	—
Total	99.74	99.66	—	—	—	—	—
FeO	7.03	6.74	—	—	—	—	—
Fe_2O_3	7.35	8.03	—	—	—	—	—
TFeO	13.64	13.97	14.50	12.22	10.97	12.13	14.87
$Mg^{\#}$	0.54	0.37	0.54	0.51	0.55	0.47	0.40

—, no information. Data sources: [1]Jiang *et al*., 2004; [2]our unpublished data; [3]Bai *et al*., 2012; [4]Zhou *et al.*, 2005; [5]Shellnutt et al., 2011; [6]Jakobsen *et al*., 2010; [7]Namur *et al.*, 2010.

Table 4

Name	Wajilitag	Puchang	Hongge[1]	Panzhihua[2]	Skaergaard[3]	Bushveld[4]	Sept Iles[5]	Kiglapait[6]	Windimurra[7]	Bjerkreim–Sokndal[8]
Olivine (Fo)	~0.77	~0.65	0.74-0.78	~0.71	~0.56	—	~0.66	~0.56	~0.58	—
Clinopyroxene ($Mg^{\#}$)	~0.83	~0.76	0.80-0.82	~0.79	~0.65	~0.67	—	~0.70	~0.67	~0.75
Plagioclase (An)	—	~0.64	—	~0.69	~0.53	~0.61	~0.61	~0.45	~0.64	~0.50

—, silicate minerals absent at the level of Fe–Ti oxide saturation. Data sources: [1]Bai *et al*., 2012; Luan *et al.*, 2014; [2]Pang *et al.*, 2009; [3]McBirney, 1996; [4]Tegner *et al*., 2006; [5]Namur *et al.*, 2010; [6]Morse, 1979; [7]Mathison & Ahmat, 1996; [8]Wilson *et al*., 1996.

Research Highlights

- The intrusive rocks were derived from subduction-related metasomatic SCLM.
- The recycled subduction–related components effect generation of Fe–rich magmas.
- External H_2O addition favors the formation of massive ores.

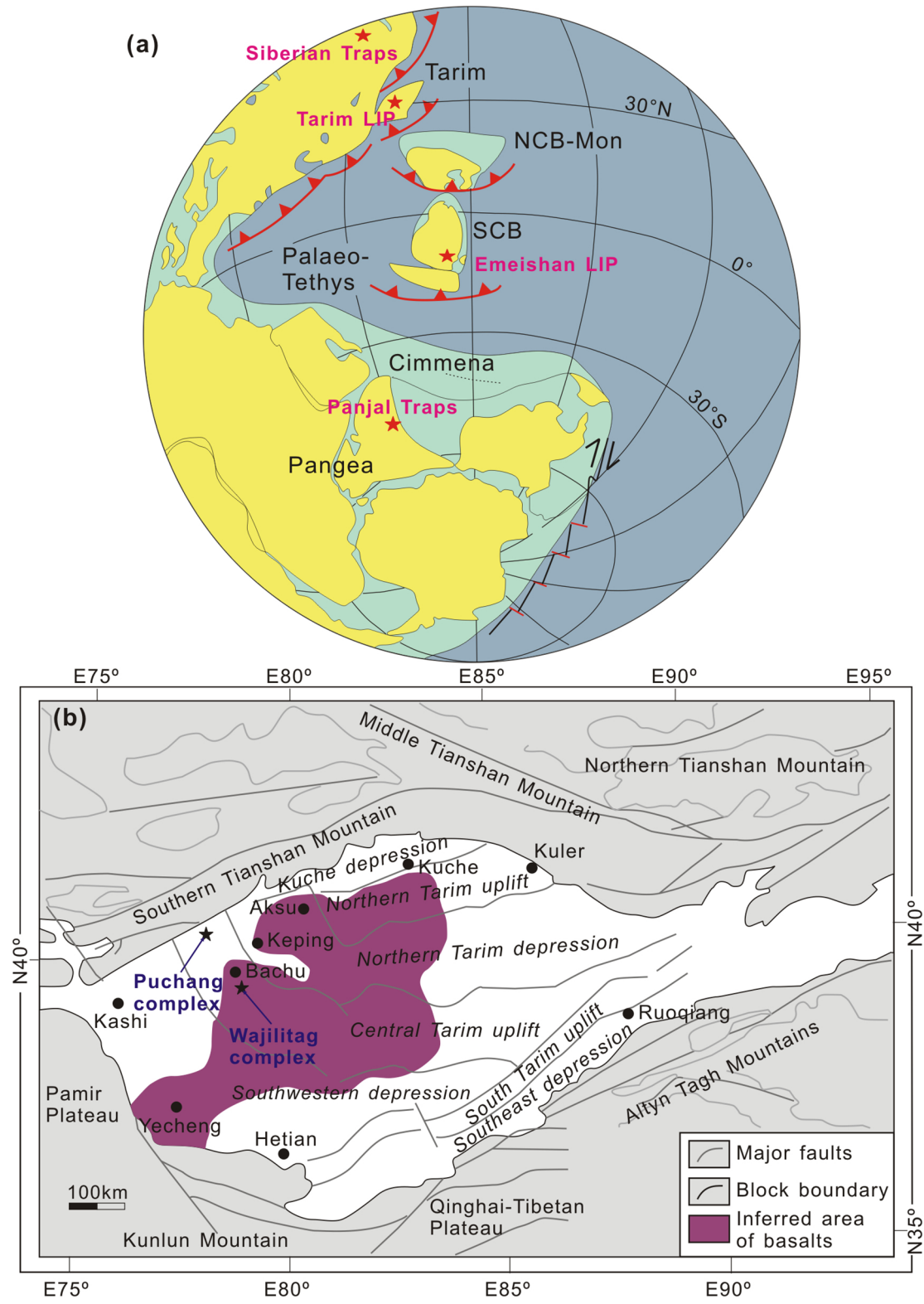
(a)
Siberian Traps
Tarim
Tarim LIP
30°N
NCB-Mon
SCB
Palaeo-
Tethys
Emeishan LIP
0°
Cimmena
Panjal Traps
30°S
Pangea
E75°
E80°
E85°
E90°
E95°
(b)
Middle Tianshan Mountain
Northern Tianshan Mountain
Southern Tianshan Mountain
Kuche depression
Kuche
Kuler
Aksu
Northern Tarim uplift
Keping
Northern Tarim depression
Bachu
Puchang
complex
Kashi
Wajilitag
complex
Central Tarim uplift
Ruoqiang
South Tarim uplift
Southeast depression
Altyn Tagh Mountains
Pamir
Plateau
Southwestern depression
Yecheng
Hetian
100km
Qinghai-Tibetan
Plateau
Kunlun Mountain
Major faults
Block boundary
Inferred area
of basalts
N40°
N35°
E75°
E80°
E85°
E90°

Figure 1

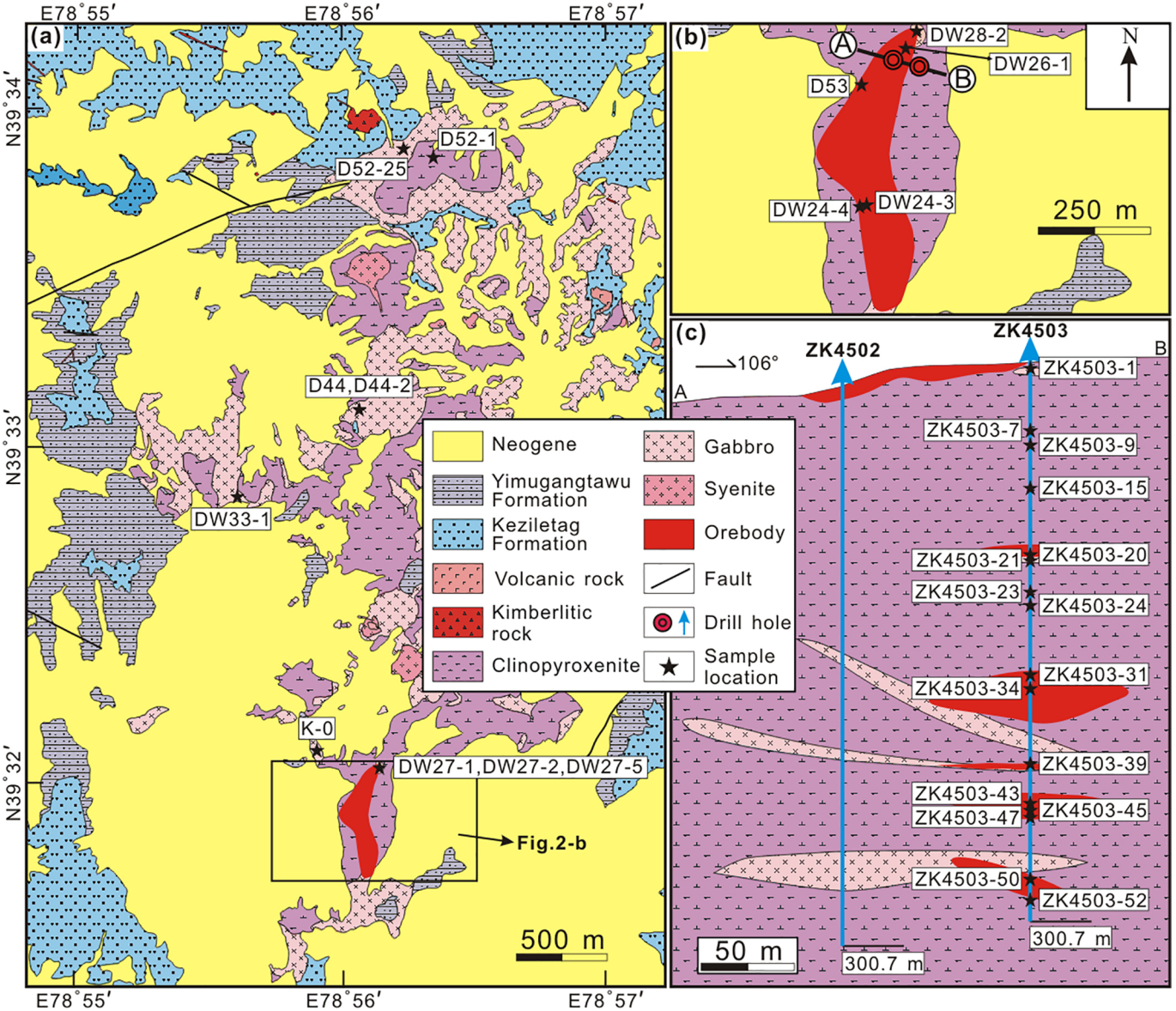
(a)
E78°55′
E78°56′
E78°57′
N39°34′
N39°33′
N39°32′
D52-1
D52-25
D44,D44-2
DW33-1
K-0
DW27-1,DW27-2,DW27-5
Fig.2-b
500 m
Neogene
Yimugangtawu Formation
Keziletag Formation
Volcanic rock
Kimberlitic rock
Clinopyroxenite
Gabbro
Syenite
Orebody
Fault
Drill hole
Sample location
(b)
A
B
DW28-2
DW26-1
D53
DW24-4
DW24-3
N
250 m
(c)
106°
ZK4502
ZK4503
A
B
ZK4503-1
ZK4503-7
ZK4503-9
ZK4503-15
ZK4503-21
ZK4503-20
ZK4503-23
ZK4503-24
ZK4503-31
ZK4503-34
ZK4503-39
ZK4503-43
ZK4503-47
ZK4503-45
ZK4503-50
ZK4503-52
300.7 m
300.7 m
50 m

Figure 2

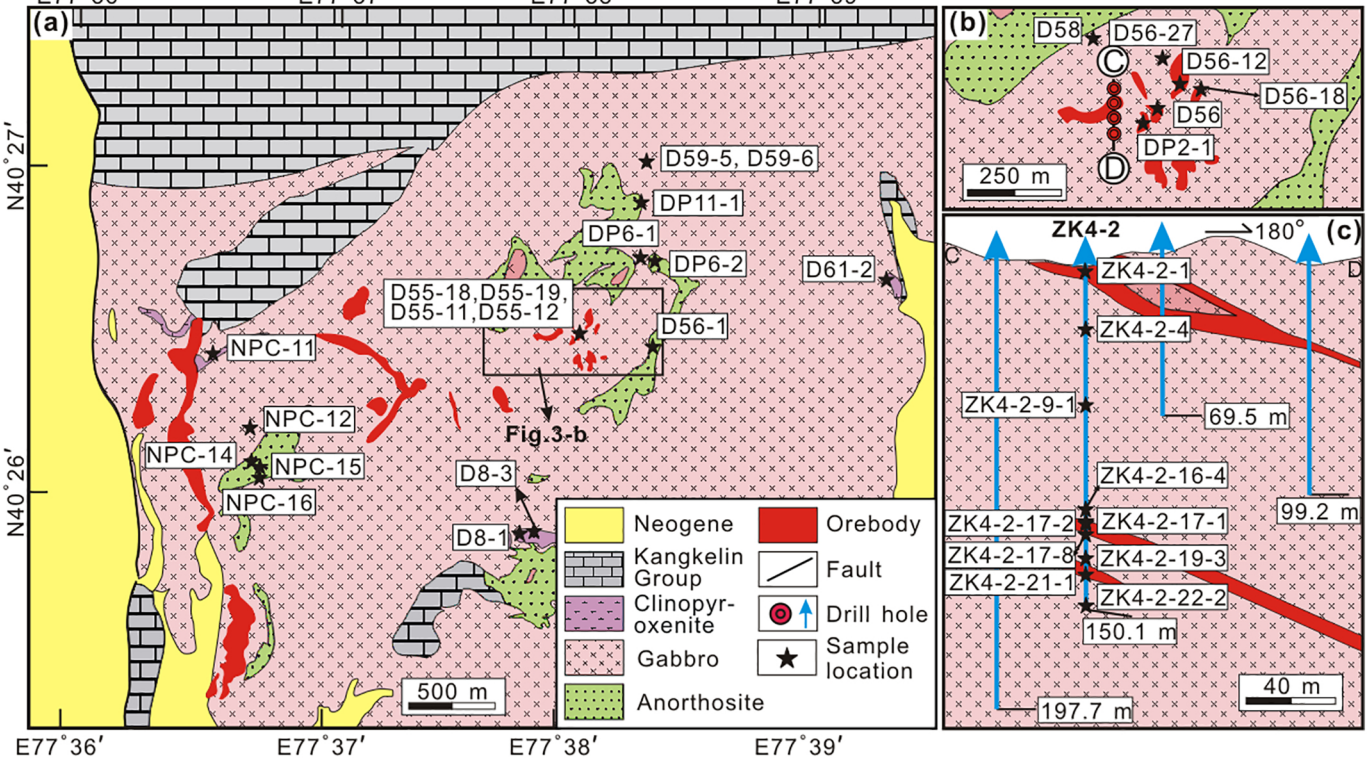
E77°36′
E77°37′
E77°38′
E77°39′
N40°27′
N40°26′
(a)
D59-5, D59-6
DP11-1
DP6-1
DP6-2
D61-2
D55-18,D55-19,
D55-11,D55-12
D56-1
NPC-11
NPC-12
NPC-14
NPC-15
NPC-16
Fig.3-b
D8-3
D8-1
500 m
Neogene
Kangkelin Group
Clinopyr-oxenite
Gabbro
Anorthosite
Orebody
Fault
Drill hole
Sample location
(b)
D58
D56-27
C
D56-12
D56-18
D56
DP2-1
D
250 m
(c)
ZK4-2
180°
C
D
ZK4-2-1
ZK4-2-4
ZK4-2-9-1
69.5 m
ZK4-2-16-4
ZK4-2-17-2
ZK4-2-17-1
99.2 m
ZK4-2-17-8
ZK4-2-19-3
ZK4-2-21-1
ZK4-2-22-2
150.1 m
40 m
197.7 m

Figure 3

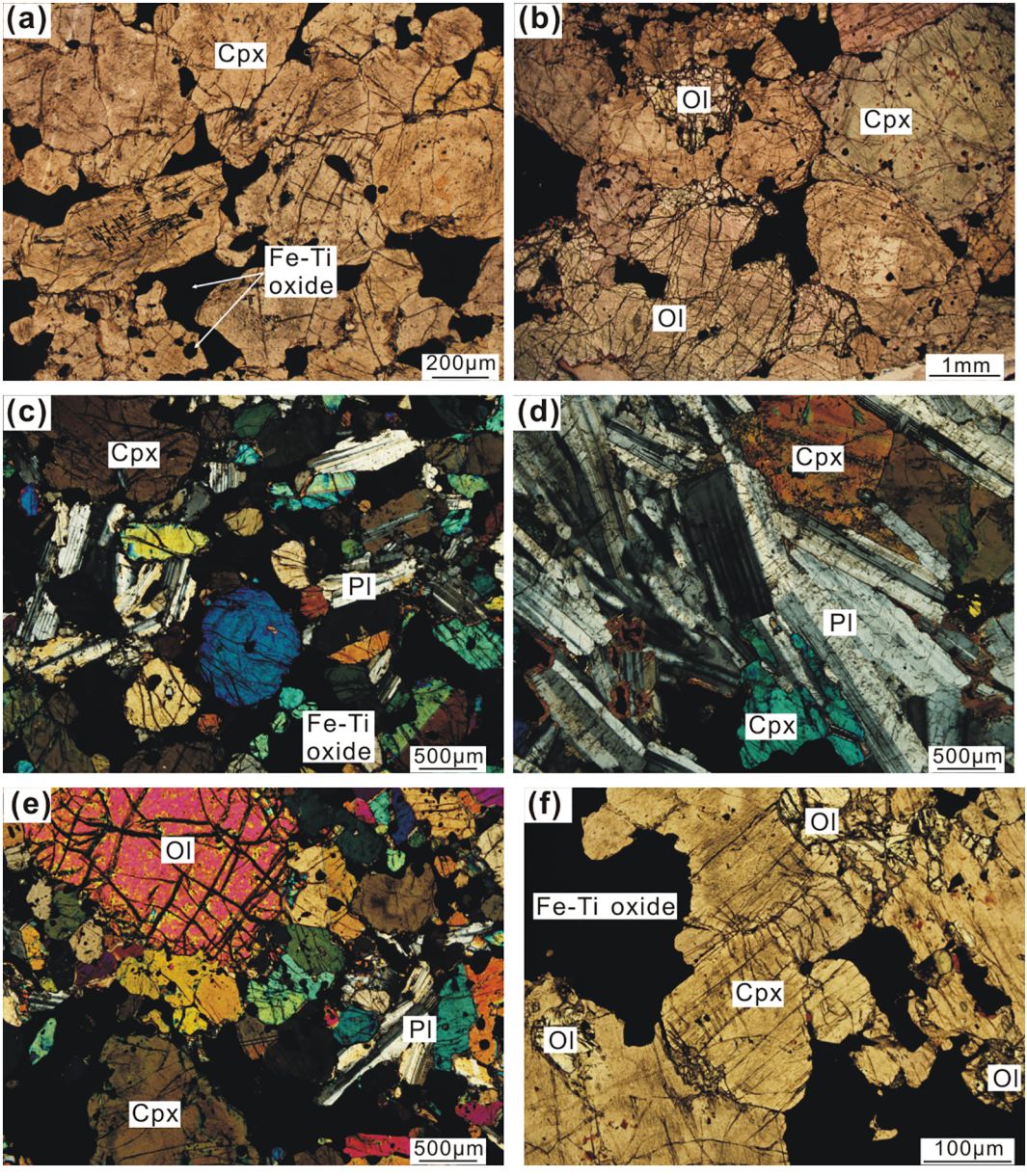
(a)
Cpx
Fe-Ti
oxide
200μm
(b)
Ol
Cpx
Ol
1mm
(c)
Cpx
Pl
Fe-Ti
oxide
500μm
(d)
Cpx
Pl
Cpx
500μm
(e)
Ol
Pl
Cpx
500μm
(f)
Ol
Fe-Ti oxide
Cpx
Ol
Ol
100μm

Figure 4

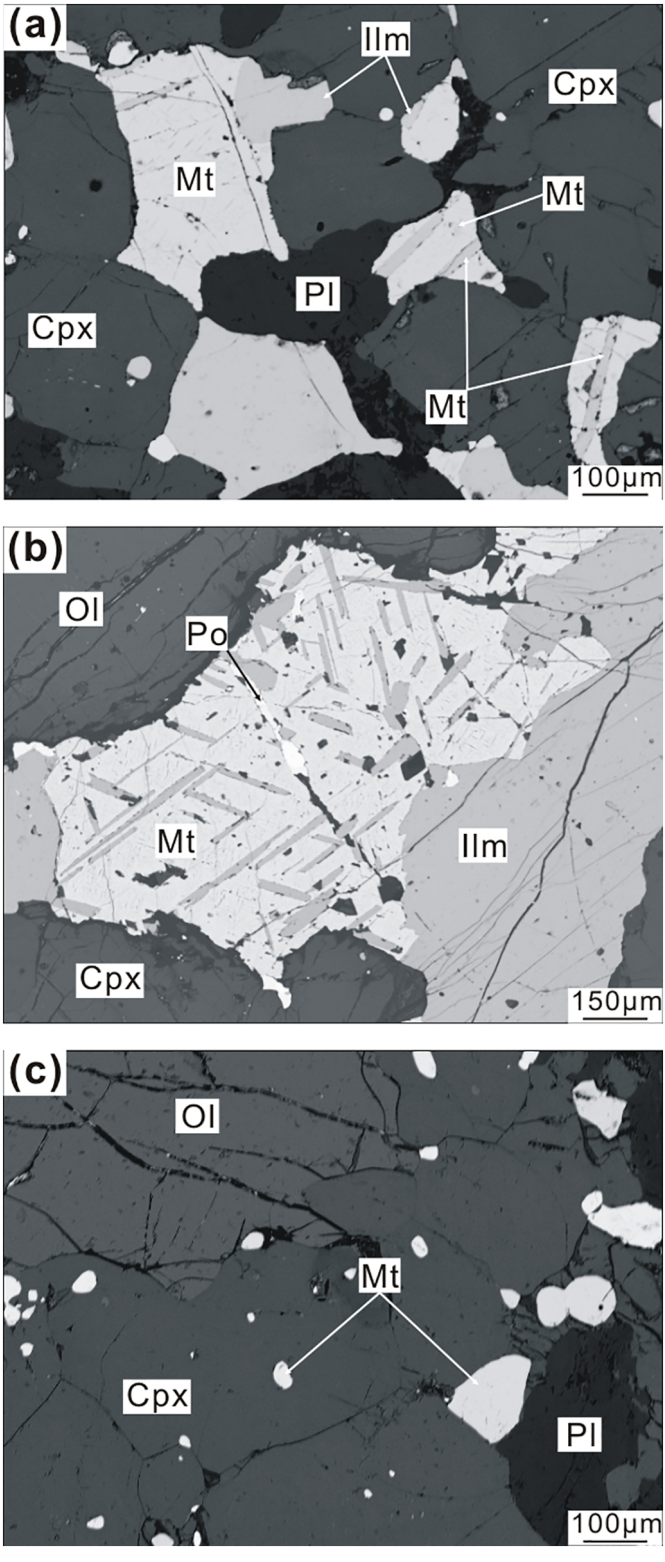
(a)
Ilm
Cpx
Mt
Mt
Pl
Cpx
Mt
100μm
(b)
Ol
Po
Mt
Ilm
Cpx
150μm
(c)
Ol
Mt
Cpx
Pl
100μm

Figure 5

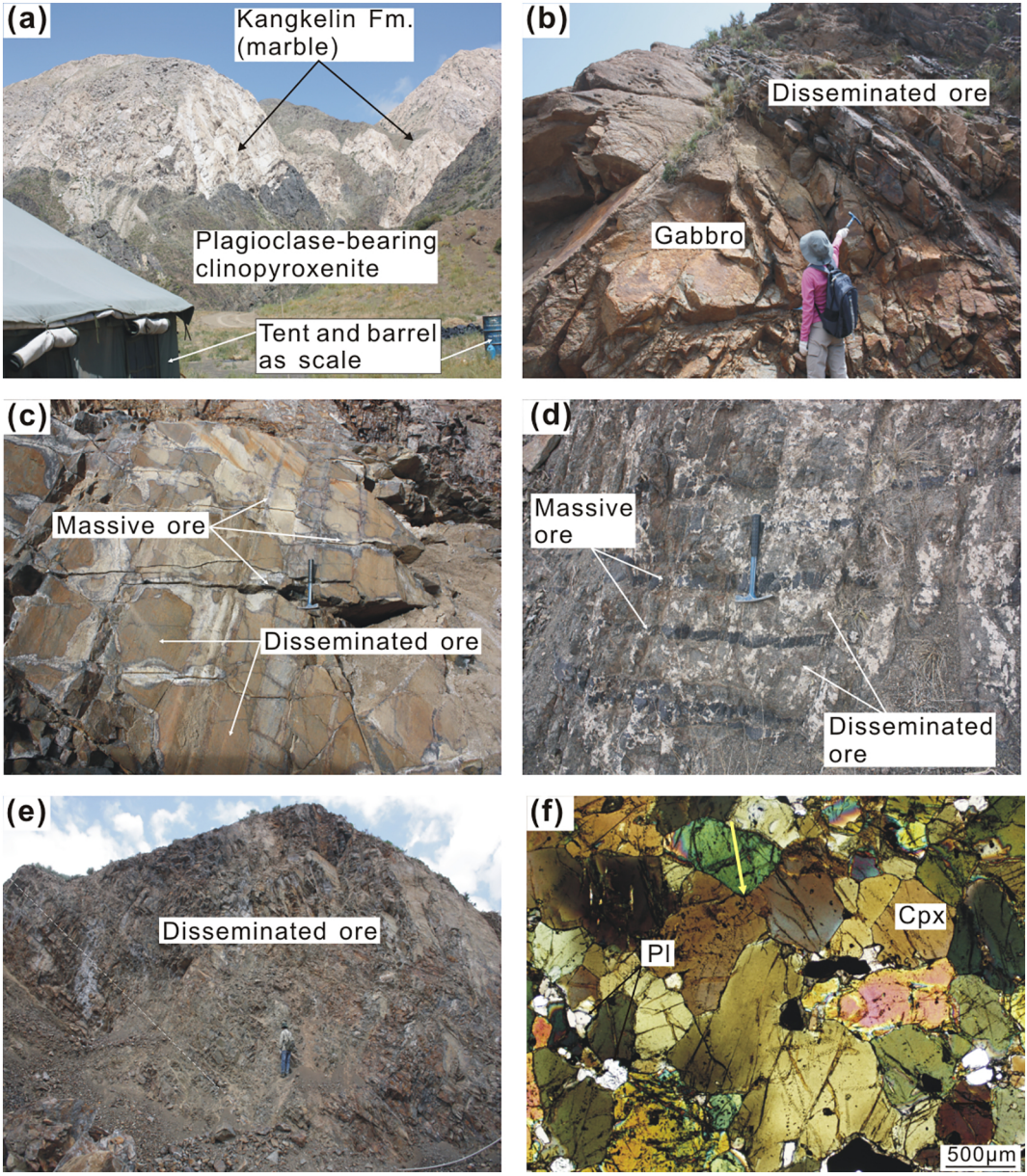
(a)
Kangkelin Fm. (marble)
Plagioclase-bearing clinopyroxenite
Tent and barrel as scale
(b)
Disseminated ore
Gabbro
(c)
Massive ore
Disseminated ore
(d)
Massive ore
Disseminated ore
(e)
Disseminated ore
(f)
Cpx
Pl
500μm

Figure 6af

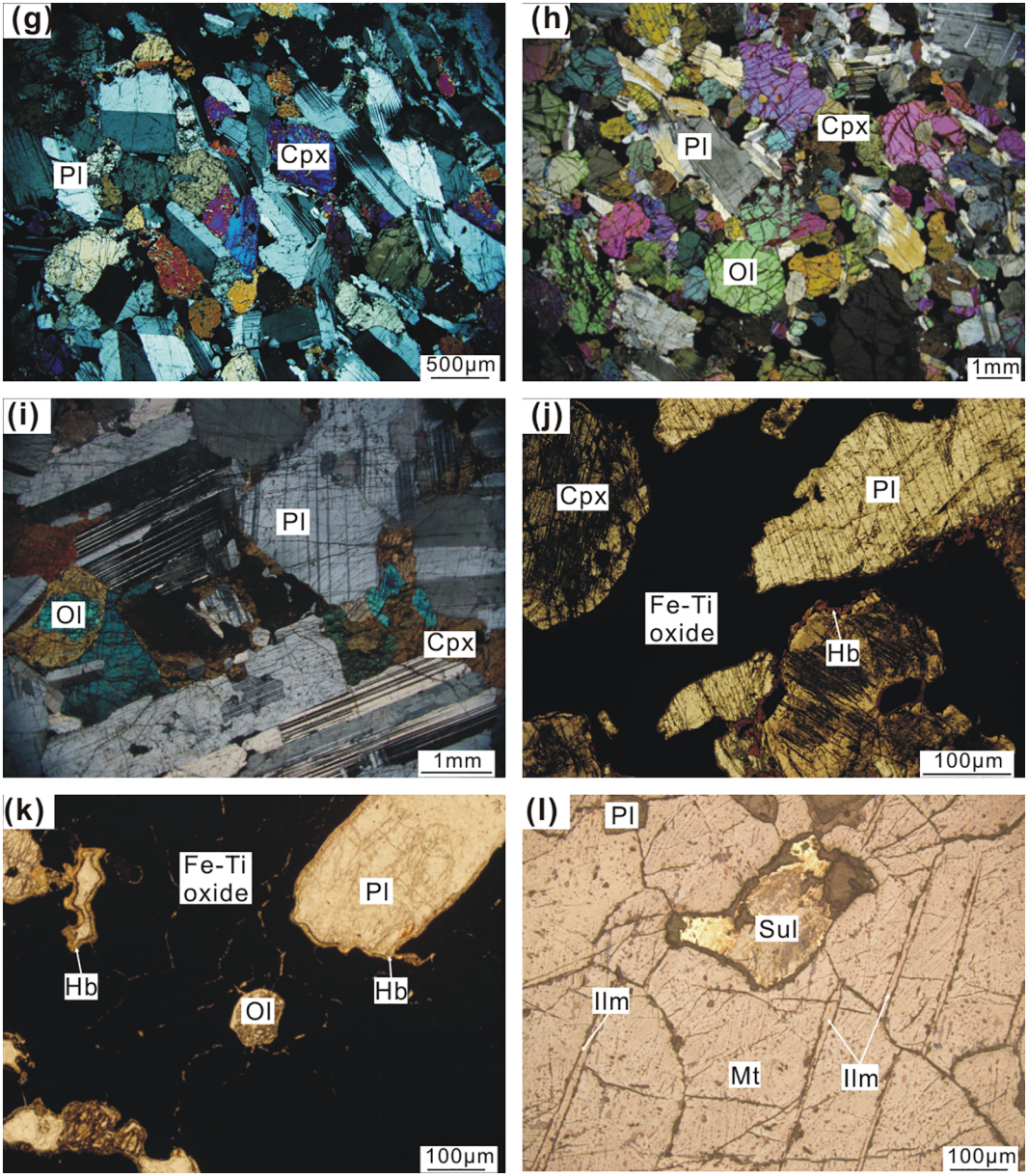
(g)
Pl
Cpx
500μm
(h)
Pl
Cpx
Ol
1mm
(i)
Pl
Ol
Cpx
1mm
(j)
Cpx
Pl
Fe-Ti
oxide
Hb
100μm
(k)
Fe-Ti
oxide
Pl
Hb
Ol
Hb
100μm
(l)
Pl
Sul
Ilm
Mt
Ilm
100μm

Figure 6gl

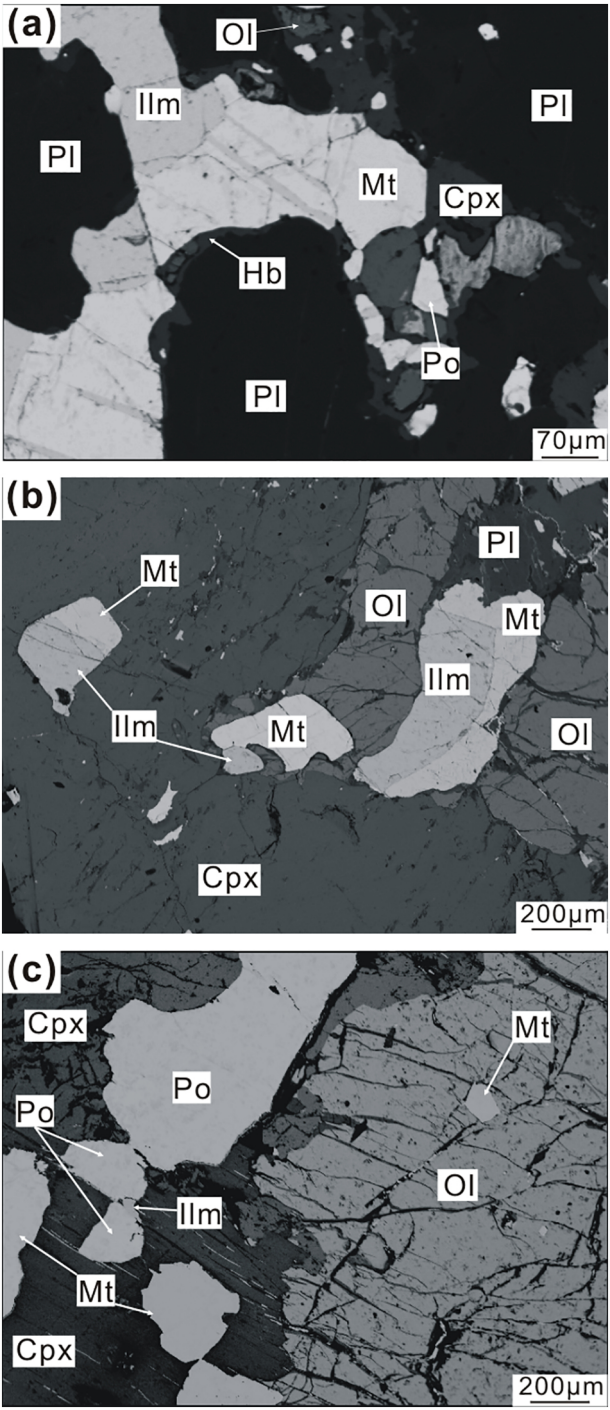
(a)
Ol
Ilm
Pl
Pl
Mt
Cpx
Hb
Po
Pl
70μm
(b)
Pl
Mt
Ol
Mt
Ilm
Ilm
Mt
Ol
Cpx
200μm
(c)
Cpx
Mt
Po
Po
Ol
Ilm
Mt
Cpx
200μm

Figure 7

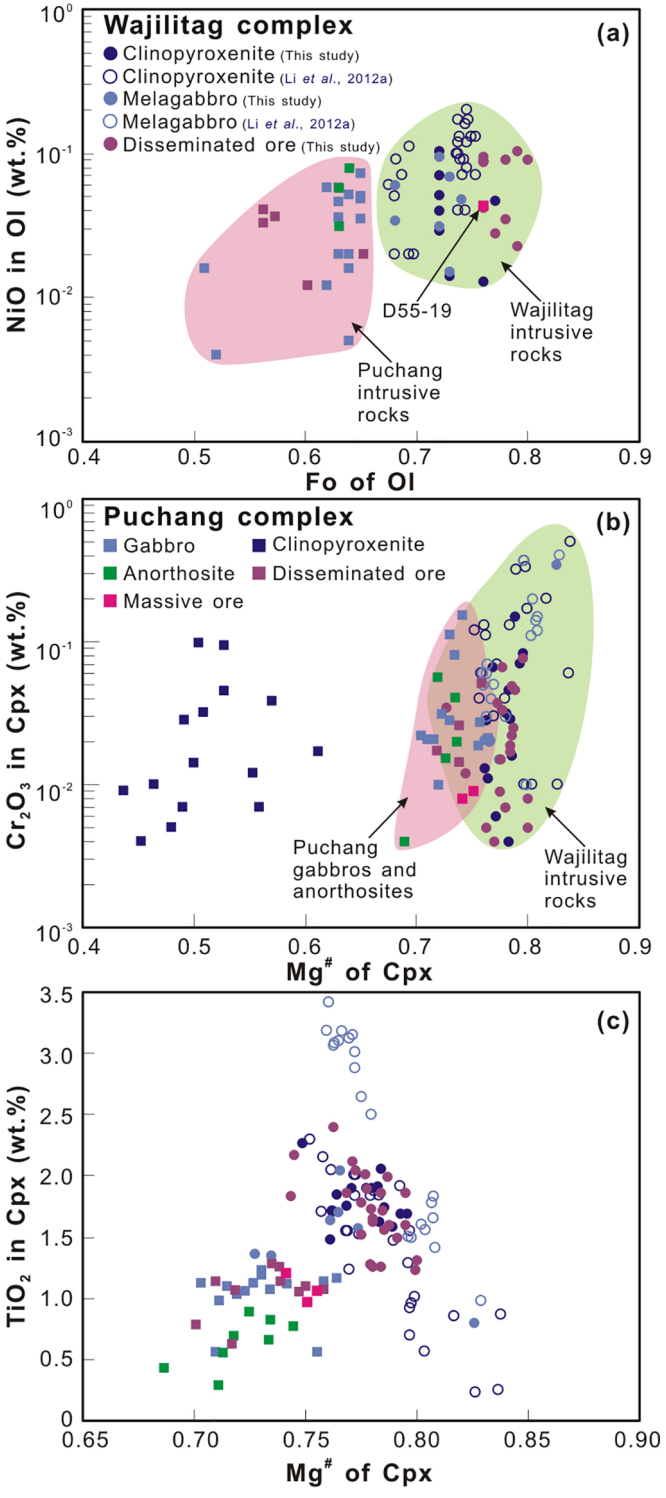
Wajilitag complex
(a)
Clinopyroxenite (This study)
Clinopyroxenite (Li et al., 2012a)
Melagabbro (This study)
Melagabbro (Li et al., 2012a)
Disseminated ore (This study)
D55-19
Wajilitag intrusive rocks
Puchang intrusive rocks
NiO in Ol (wt.%)
Fo of Ol
Puchang complex
(b)
Gabbro
Clinopyroxenite
Anorthosite
Disseminated ore
Massive ore
Puchang gabbros and anorthosites
Wajilitag intrusive rocks
Cr2O3 in Cpx (wt.%)
Mg# of Cpx
(c)
TiO2 in Cpx (wt.%)
Mg# of Cpx

Figure 8

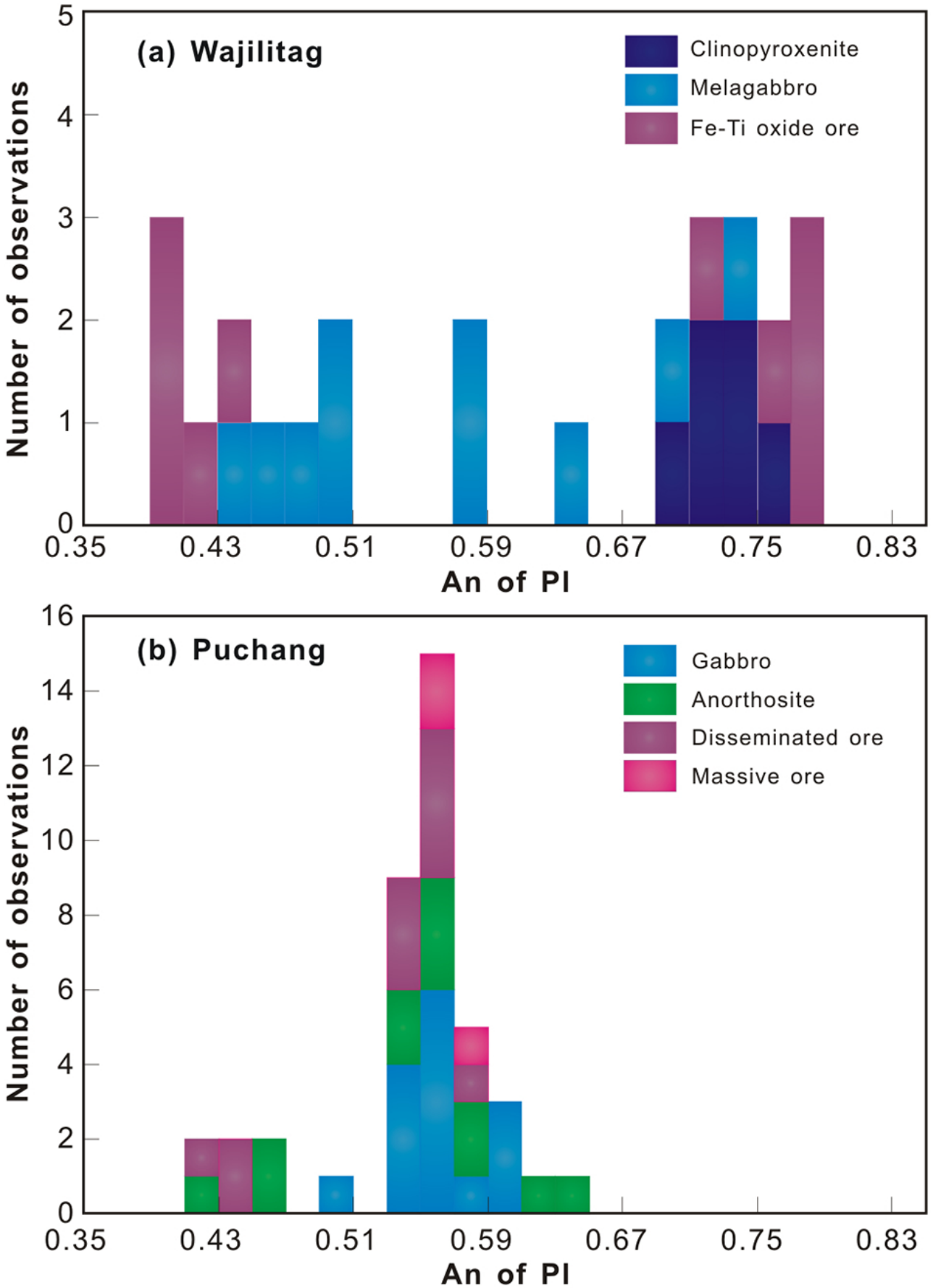
(a) Wajilitag
Clinopyroxenite
Melagabbro
Fe-Ti oxide ore
Number of observations
0
1
2
3
4
5
0.35
0.43
0.51
0.59
0.67
0.75
0.83
An of Pl
(b) Puchang
Gabbro
Anorthosite
Disseminated ore
Massive ore
Number of observations
0
2
4
6
8
10
12
14
16
0.35
0.43
0.51
0.59
0.67
0.75
0.83
An of Pl

Figure 9

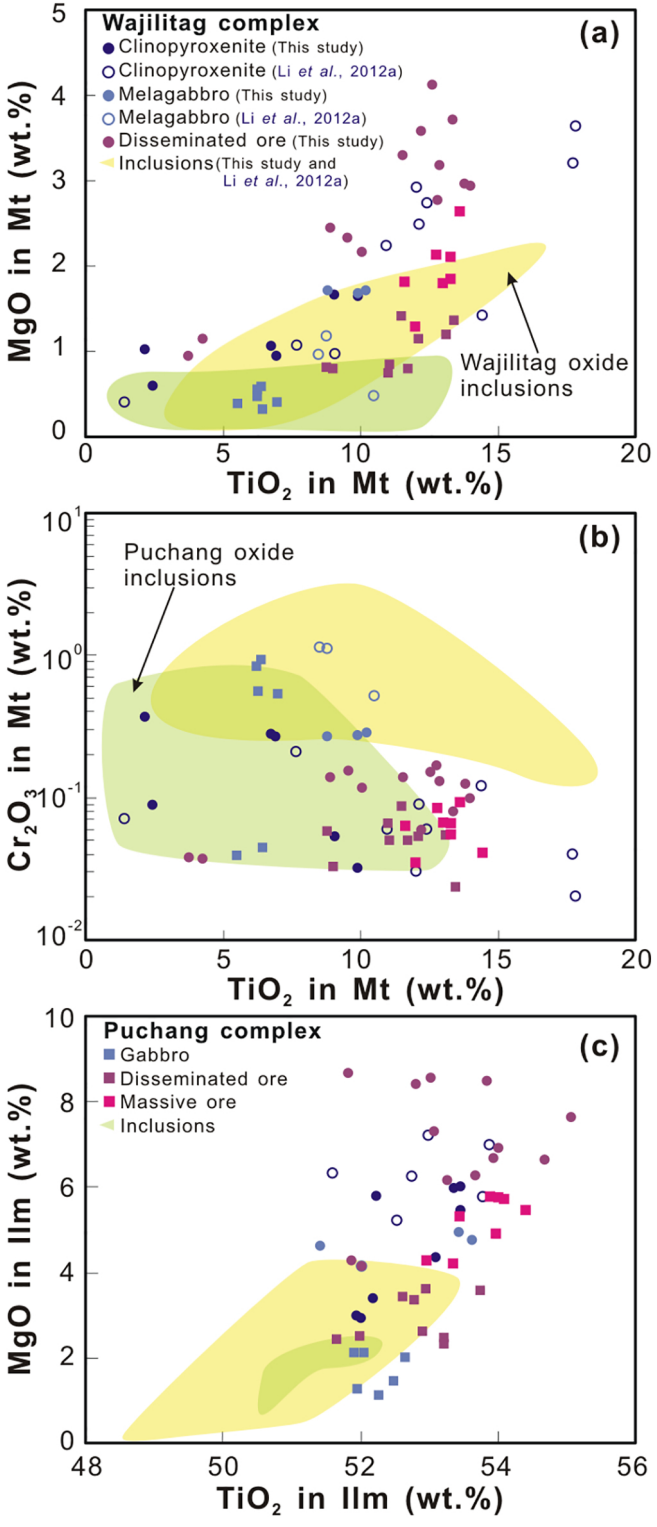
Wajilitag complex
Clinopyroxenite (This study)
Clinopyroxenite (Li et al., 2012a)
Melagabbro (This study)
Melagabbro (Li et al., 2012a)
Disseminated ore (This study)
Inclusions (This study and Li et al., 2012a)
(a)
MgO in Mt (wt.%)
TiO2 in Mt (wt.%)
Wajilitag oxide inclusions
(b)
Puchang oxide inclusions
Cr2O3 in Mt (wt.%)
TiO2 in Mt (wt.%)
Puchang complex
Gabbro
Disseminated ore
Massive ore
Inclusions
(c)
MgO in Ilm (wt.%)
TiO2 in Ilm (wt.%)

Figure 10

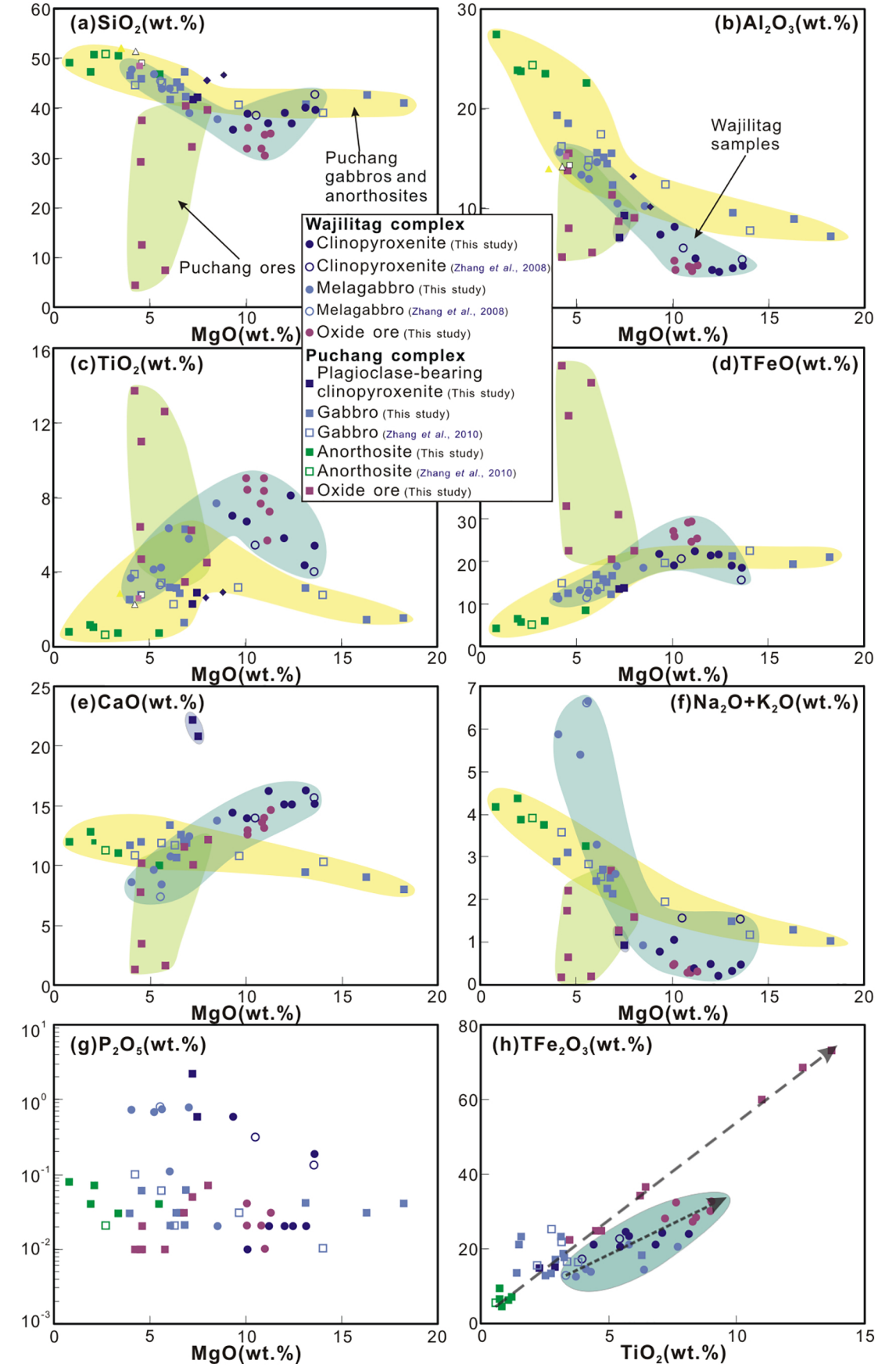
(a)SiO2(wt.%)
(b)Al2O3(wt.%)
(c)TiO2(wt.%)
(d)TFeO(wt.%)
(e)CaO(wt.%)
(f)Na2O+K2O(wt.%)
(g)P2O5(wt.%)
(h)TFe2O3(wt.%)
MgO(wt.%)
TiO2(wt.%)
Puchang gabbros and anorthosites
Puchang ores
Wajilitag samples
Wajilitag complex
Clinopyroxenite (This study)
Clinopyroxenite (Zhang et al., 2008)
Melagabbro (This study)
Melagabbro (Zhang et al., 2008)
Oxide ore (This study)
Puchang complex
Plagioclase-bearing clinopyroxenite (This study)
Gabbro (This study)
Gabbro (Zhang et al., 2010)
Anorthosite (This study)
Anorthosite (Zhang et al., 2010)
Oxide ore (This study)

Figure 11

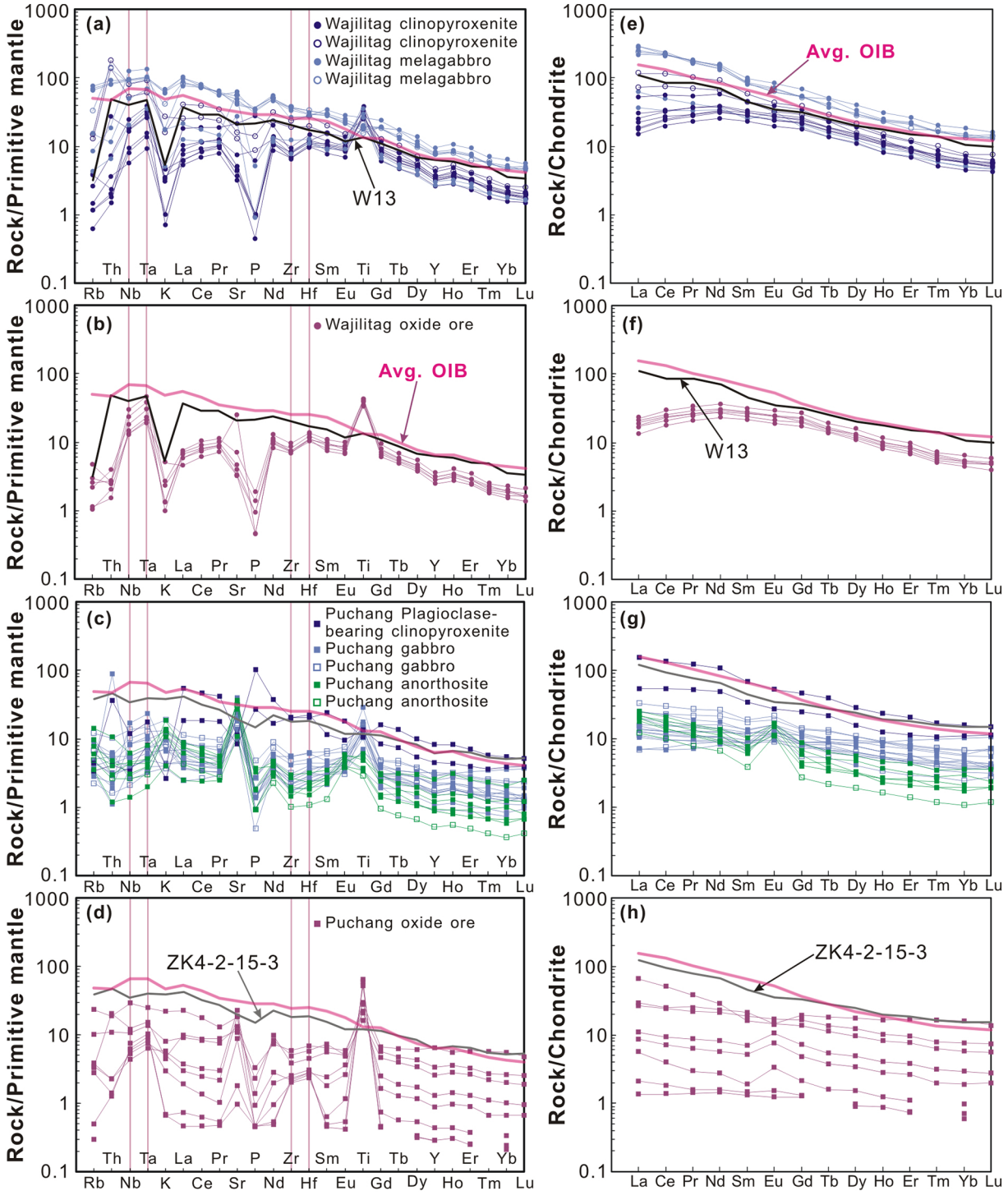
(a)
Wajilitag clinopyroxenite
Wajilitag clinopyroxenite
Wajilitag melagabbro
Wajilitag melagabbro
W13
(b)
Wajilitag oxide ore
Avg. OIB
(c)
Puchang Plagioclase-bearing clinopyroxenite
Puchang gabbro
Puchang gabbro
Puchang anorthosite
Puchang anorthosite
(d)
Puchang oxide ore
ZK4-2-15-3
(e)
Avg. OIB
(f)
W13
(g)
(h)
ZK4-2-15-3
Rock/Primitive mantle
Rock/Chondrite
Rb Nb K Ce Sr Nd Hf Eu Gd Dy Ho Tm Lu
Th Ta La Pr P Zr Sm Ti Tb Y Er Yb
La Ce Pr Nd Sm Eu Gd Tb Dy Ho Er Tm Yb Lu
1000
100
10
1
0.1

Figure 12

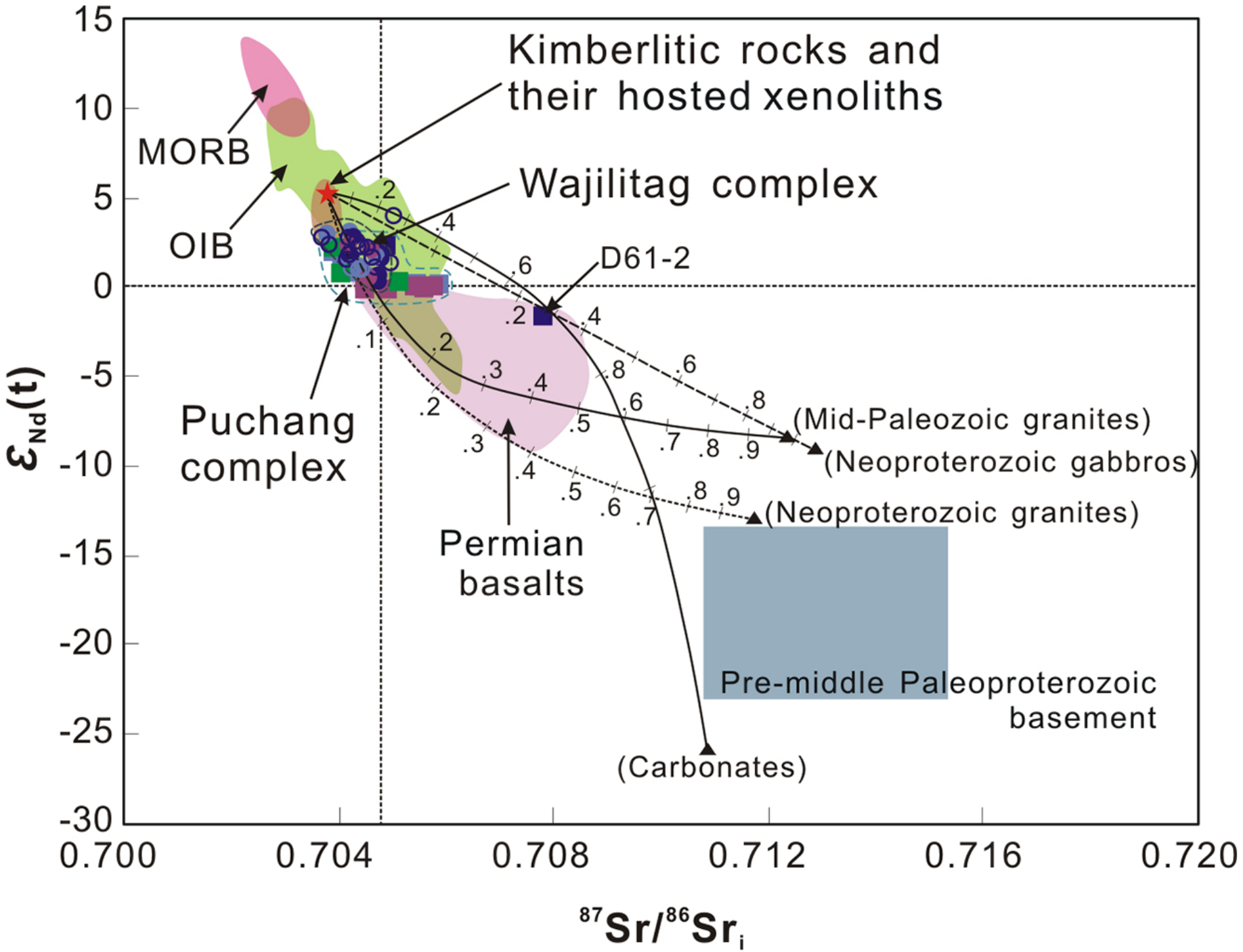
Kimberlitic rocks and their hosted xenoliths
MORB
OIB
Wajilitag complex
D61-2
Puchang complex
Permian basalts
(Mid-Paleozoic granites)
(Neoproterozoic gabbros)
(Neoproterozoic granites)
(Carbonates)
Pre-middle Paleoproterozoic basement
$\varepsilon_{Nd}(t)$
$^{87}Sr/^{86}Sr_i$
15
10
5
0
-5
-10
-15
-20
-25
-30
0.700
0.704
0.708
0.712
0.716
0.720

Figure 13

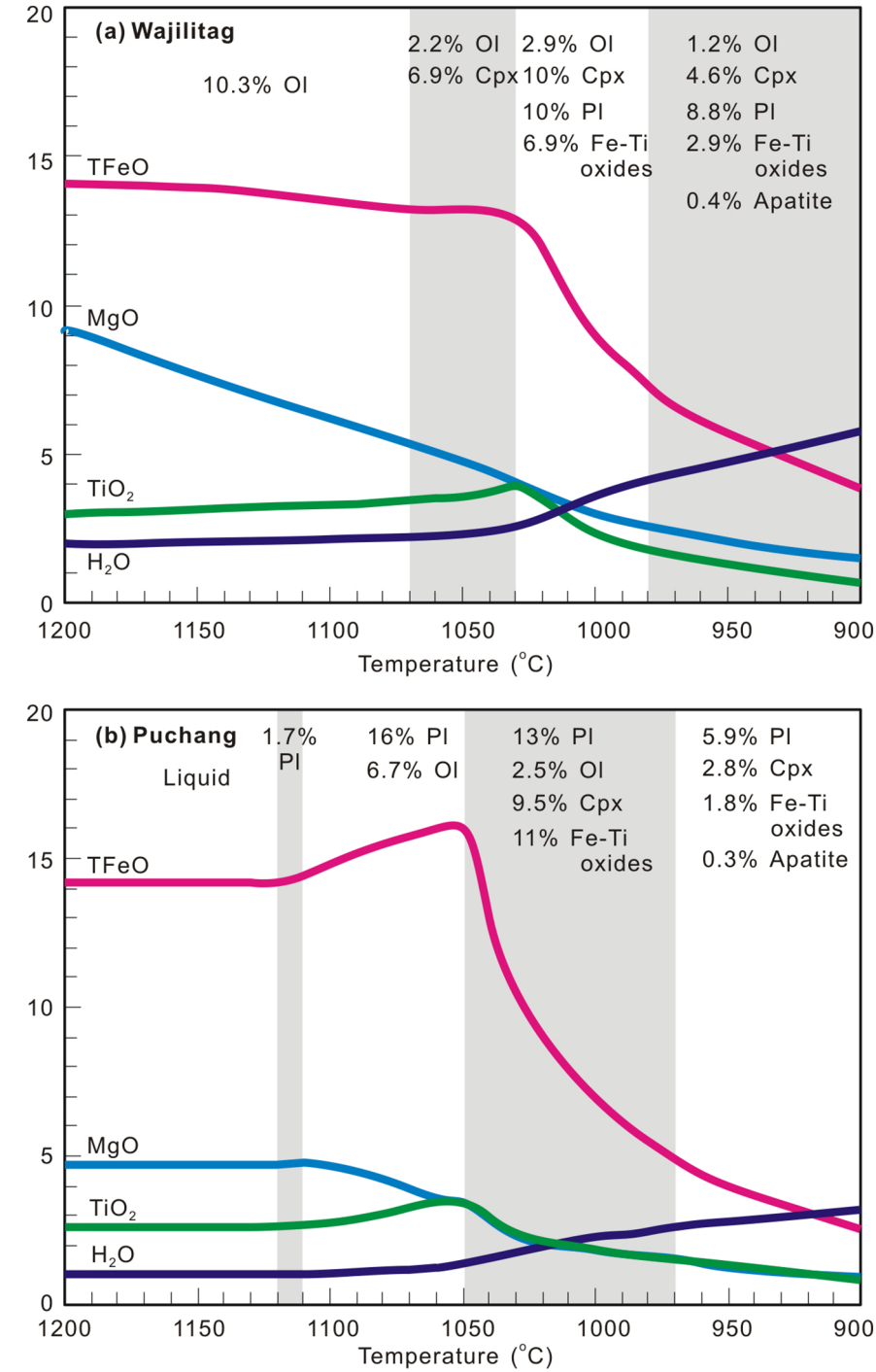
(a) Wajilitag
10.3% Ol
2.2% Ol
6.9% Cpx
2.9% Ol
10% Cpx
10% Pl
6.9% Fe-Ti oxides
1.2% Ol
4.6% Cpx
8.8% Pl
2.9% Fe-Ti oxides
0.4% Apatite
TFeO
MgO
TiO2
H2O
20
15
10
5
0
1200
1150
1100
1050
1000
950
900
Temperature (°C)
(b) Puchang
Liquid
1.7% Pl
16% Pl
6.7% Ol
13% Pl
2.5% Ol
9.5% Cpx
11% Fe-Ti oxides
5.9% Pl
2.8% Cpx
1.8% Fe-Ti oxides
0.3% Apatite
TFeO
MgO
TiO2
H2O
20
15
10
5
0
1200
1150
1100
1050
1000
950
900
Temperature (°C)

Figure 14

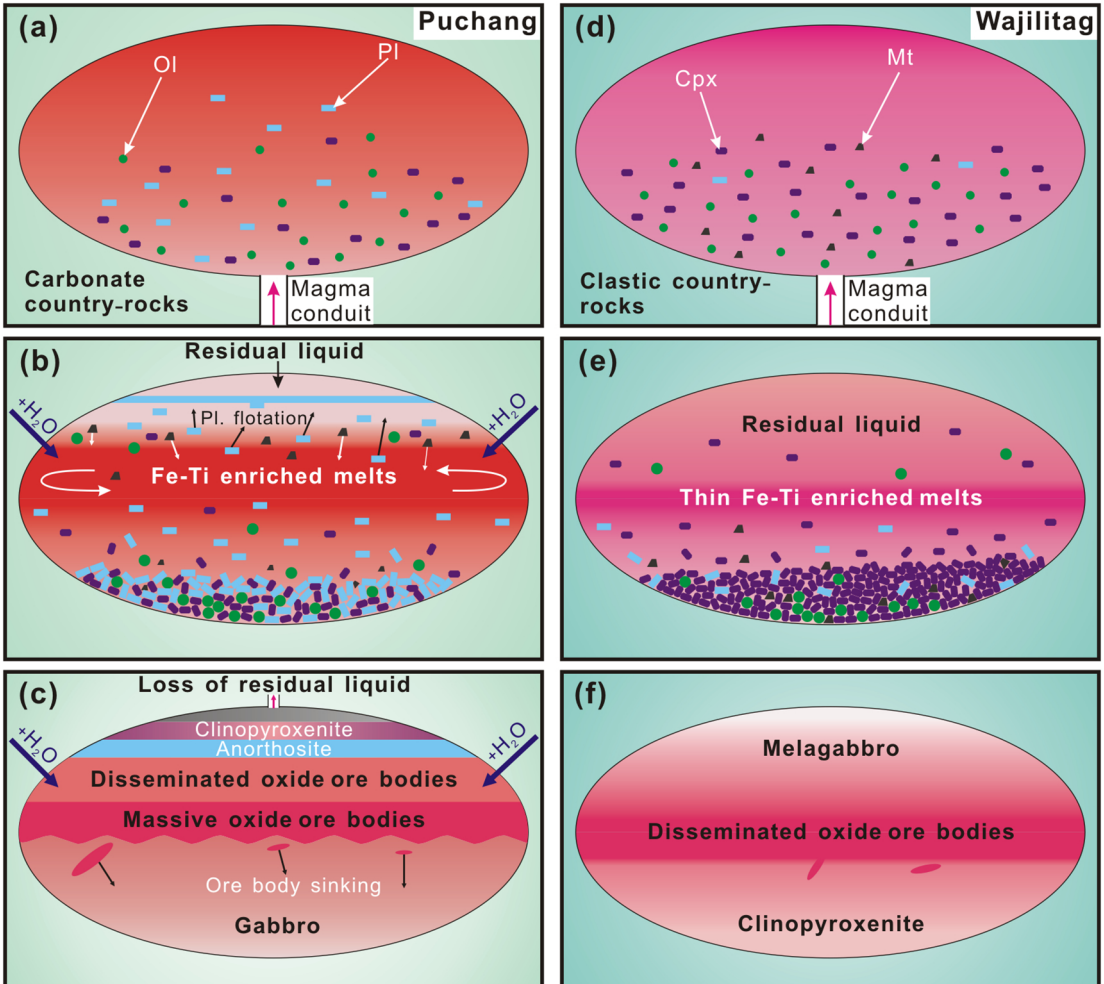
(a)
Puchang
Ol
Pl
Carbonate country-rocks
Magma conduit
(d)
Wajilitag
Cpx
Mt
Clastic country-rocks
Magma conduit
(b)
Residual liquid
+H2O
Pl. flotation
+H2O
Fe-Ti enriched melts
(e)
Residual liquid
Thin Fe-Ti enriched melts
(c)
Loss of residual liquid
+H2O
Clinopyroxenite
Anorthosite
+H2O
Disseminated oxide ore bodies
Massive oxide ore bodies
Ore body sinking
Gabbro
(f)
Melagabbro
Disseminated oxide ore bodies
Clinopyroxenite

Figure 15